Supplementary Information

Mechanistic Insights into pH-Dependent Ofloxacin Adsorption on Nanoporous Carbons

Fatokhoma A. Camara[†], Hamidréza Ramézani[†]*, Nathalie Mathieu[†], Sandrine Delpeux-Ouldriane[†] and Suresh K. Bhatia[‡]

[†]*Université d'Orléans, CNRS, ICMN, UMR 7374, 3 avenue de la Recherche Scientifique, 45071 Orléans cedex 2, France*
[‡]*School of Chemical Engineering, The University of Queensland, Brisbane, QLD 4072, Australia*

Corresponding author: Hamidréza Ramézani **E-mail:** hamidreza.ramezani@univ-orleans.fr **Phone:** +33 2 38 257879

Supporting information submitted to RSC, March 4, 2026

1 Ofloxacin force field

1.1 Neutral HQ^0 and basic Q^- forms of ofloxacin

The force field parameters for ofloxacin molecules in both neutral and charged cases were optimized using the GGA:BP86 functional and the TZP subset. The computed structure of ofloxacin was then employed to generate the force field using LigPargen. The non-bonded force field parameters for HQ^0 and Q^- are reported in Table S1.

Table S1 Force field parameters of HQ^0, and Q^- of ofloxacin.

Ofloxacin (HQ^0)†							Ofloxacin (Q^-)‡						
No.	**Atom ID**	**Atom label**	**σ (Å)**	**ε (kJ/mol)**	**ε/k_B (K)**	**Charge (e)**	**No.**	**Atom ID**	**Atom label**	**σ (Å)**	**ε (kJ/mol)**	**ε/k_B (K)**	**Charge (e)**
1	H14	H0O_TYPE1	2.50	0.12552	15.09659	0.11240	1	C7	C01_TYPE2	3.55	0.29288	35.22563	-0.02080
2	H5	H0Z_TYPE1	2.50	0.12552	15.09659	0.10350	2	H3	H0P_TYPE2	2.50	0.12552	15.09670	0.10230
3	C5	C0A_TYPE1	3.50	0.33472	40.25756	-0.16640	3	O4	O0M_TYPE2	2.96	0.87864	105.67690	-0.38260
4	H15	H1A_TYPE1	2.50	0.12552	15.09659	0.08450	4	C1	C02_TYPE2	3.55	0.29288	35.22563	0.15740
5	H16	H19_TYPE1	2.50	0.12552	15.09659	0.08450	5	C15	C0R_TYPE2	3.55	0.31798	38.24497	0.03510
6	H6	H0W_TYPE1	2.50	0.12552	15.09659	0.10840	6	H19	H14_TYPE2	2.50	0.12552	15.09670	0.08420
7	C11	C0V_TYPE1	3.50	0.27614	33.21249	0.08980	7	H17	H16_TYPE2	2.50	0.12552	15.09670	0.08420
8	C13	C11_TYPE1	3.50	0.27614	33.21249	0.00350	8	H16	H18_TYPE2	2.50	0.12552	15.09670	0.06680
9	N2	N0T_TYPE1	3.30	0.71128	85.54732	-0.70040	9	H12	H10_TYPE2	2.42	0.12552	15.09670	0.15470
10	H11	H12_TYPE1	2.50	0.12552	15.09659	0.09640	10	H8	H0T_TYPE2	2.50	0.12552	15.09670	0.07830
11	F1	F0S_TYPE1	2.90	0.25104	30.19317	-0.09450	11	H4	H0G_TYPE2	2.50	0.12552	15.09670	0.08860
12	C2	C0B_TYPE1	3.50	0.33472	40.25756	0.13160	12	C12	C0B_TYPE2	3.50	0.27614	33.21274	0.06640
13	C1	C0M_TYPE1	3.55	0.29288	35.22537	0.22810	13	C17	C11_TYPE2	3.50	0.27614	33.21274	-0.03860
14	C18	C0G_TYPE1	3.50	0.27614	33.21249	-0.25910	14	H9	H0S_TYPE2	2.50	0.12552	15.09670	0.07830
15	C7	C0J_TYPE1	3.55	0.29288	35.22537	0.01300	15	F1	F00_TYPE2	2.90	0.25104	30.19340	-0.11410
16	O1	O0K_TYPE1	2.90	0.58576	70.45073	-0.28270	16	C13	C0H_TYPE2	3.50	0.27614	33.21274	0.00420
17	N1	N08_TYPE1	3.25	0.71128	85.54732	-0.50000	17	C8	C0C_TYPE2	3.55	0.29288	35.22563	0.36750
18	H19	H0N_TYPE1	2.50	0.12552	15.09659	0.11240	18	C3	C04_TYPE2	3.55	0.29288	35.22563	0.02060
19	C15	C05_TYPE1	3.55	0.31798	38.24468	0.21810	19	C9	C0X_TYPE2	3.55	0.29288	35.22563	0.49010
20	O2	O01_TYPE1	3.12	0.71128	85.54732	-0.49280	20	O1	O08_TYPE2	2.90	0.58576	70.45127	-0.26090
21	C10	C0H_TYPE1	3.50	0.27614	33.21249	-0.01870	21	H18	H15_TYPE2	2.50	0.12552	15.09670	0.08420
22	C17	C17_TYPE1	3.50	0.27614	33.21249	-0.04790	22	H7	H0J_TYPE2	2.50	0.12552	15.09670	0.09060
23	H2	H0Q_TYPE1	2.50	0.12552	15.09659	0.13620	23	C4	C0Q_TYPE2	3.50	0.27614	33.21274	0.08010
24	H12	H07_TYPE1	2.42	0.12552	15.09659	0.20540	24	C18	C0Z_TYPE2	3.50	0.27614	33.21274	-0.22660
25	H8	H15_TYPE1	2.50	0.12552	15.09659	0.09650	25	N3	N0U_TYPE2	3.30	0.71128	85.54796	-0.51730
26	H1	H0F_TYPE1	2.50	0.12552	15.09659	0.13120	26	H6	H0I_TYPE2	2.50	0.12552	15.09670	0.09060
27	H7	H0X_TYPE1	2.50	0.12552	15.09659	0.10840	27	C6	C0N_TYPE2	3.55	0.31798	38.24497	-0.18980
28	H3	H0R_TYPE1	2.50	0.12552	15.09659	0.13620	28	H10	H0W_TYPE2	2.50	0.12552	15.09670	0.07800
29	C6	C03_TYPE1	3.55	0.31798	38.24468	-0.34720	29	C5	C07_TYPE2	3.50	0.33472	40.25787	-0.16280
30	C4	C0C_TYPE1	3.50	0.27614	33.21249	0.08070	30	C14	C0K_TYPE2	3.50	0.27614	33.21274	0.00300
31	C8	C06_TYPE1	3.55	0.29288	35.22537	0.44010	31	H11	H0V_TYPE2	2.50	0.12552	15.09670	0.07800
32	H4	H10_TYPE1	2.50	0.12552	15.09659	0.10350	32	C11	C0A_TYPE2	3.50	0.27614	33.21274	0.06660
33	C14	C0Y_TYPE1	3.50	0.27614	33.21249	0.00270	33	H1	H0Y_TYPE2	2.50	0.12552	15.09670	0.11170
34	O4	O09_TYPE1	2.96	0.87864	105.67610	-0.39760	34	H2	H0O_TYPE2	2.50	0.12552	15.09670	0.10230
35	C16	C0D_TYPE1	3.55	0.31798	38.24468	-0.09900	35	H13	H06_TYPE2	2.42	0.12552	15.09670	0.17180
36	H18	H00_TYPE1	0.00	0.00000	0.00000	0.43900	36	H14	H19_TYPE2	2.50	0.12552	15.09670	0.06680
37	H20	H0P_TYPE1	2.50	0.12552	15.09659	0.11240	37	C16	C03_TYPE2	3.55	0.31798	38.24497	-0.08120
38	H10	H13_TYPE1	2.50	0.12552	15.09659	0.09640	38	C10	C0D_TYPE2	3.50	0.27614	33.21274	-0.00710
39	C9	C02_TYPE1	3.55	0.29288	35.22537	0.51330	39	N2	N05_TYPE2	3.30	0.71128	85.54796	-0.57750
40	C3	C0E_TYPE1	3.55	0.29288	35.22537	0.04300	40	H5	H0F_TYPE2	2.50	0.12552	15.09670	0.08860
41	H13	H0I_TYPE1	2.42	0.12552	15.09659	0.20760	41	O2	O13_TYPE2	2.96	0.87864	105.67690	-0.58430
42	C12	C0U_TYPE1	3.50	0.27614	33.21249	0.08690	42	C2	C09_TYPE2	3.50	0.33472	40.25787	0.16380
43	H9	H16_TYPE1	2.50	0.12552	15.09659	0.09650	43	N1	N0E_TYPE2	3.25	0.71128	85.54796	-0.47350
44	O3	O04_TYPE1	2.96	0.87864	105.67610	-0.51310	44	H15	H17_TYPE2	2.50	0.12552	15.09670	0.06680
45	H17	H18_TYPE1	2.50	0.12552	15.09659	0.08450	45	O3	O12_TYPE2	2.96	0.87864	105.67690	-0.58430
46	N3	N14_TYPE1	3.30	0.71128	85.54732	-0.58710	-	-	-	-	-	-	-
47	-	-	-	-	-	-	-	-	-	-	-	-	-

1.2 Acidic H_2Q^+ and zwitterionic $HQ^{\pm}$ forms of ofloxacin

The non-bonded force field parameters of H_2Q^+ and $HQ^{\pm}$ are also reported in Table S2.

Table S2 Force field parameters of H_2Q^+, and $HQ^{\pm}$ of ofloxacin.

Ofloxacin (H_2Q^+)†							Ofloxacin ($HQ^{\pm}$)‡						
No.	Atom ID	Atom label	σ (Å)	ε (kJ/mol)	ε/k_B (K)	Charge (e)	No.	Atom ID	Atom label	σ (Å)	ε (kJ/mol)	ε/k_B (K)	Charge (e)
1	N3	N14_TYPE3	3.25	0.71128	85.54796	-0.17130	1	H17	H1A_TYPE4	2.50	0.12552	15.09670	0.15520
2	H10	H0X_TYPE3	2.50	0.12552	15.09670	0.12560	2	C9	C0X_TYPE4	3.55	0.29288	35.22563	0.55390
3	H4	H0R_TYPE3	2.50	0.12552	15.09670	0.12480	3	C18	C0Z_TYPE4	3.50	0.27614	33.21274	-0.25630
4	C14	C11_TYPE3	3.50	0.27614	33.21274	-0.08250	4	H10	H0I_TYPE4	2.50	0.12552	15.09670	0.14230
5	O3	O04_TYPE3	2.96	0.87864	105.67690	-0.42700	5	H19	H16_TYPE4	2.50	0.12552	15.09670	0.10530
6	H20	H0P_TYPE3	2.50	0.12552	15.09670	0.10130	6	O1	O08_TYPE4	2.90	0.58576	70.45127	-0.29980
7	C18	C0G_TYPE3	3.50	0.27614	33.21274	-0.22880	7	H7	H0T_TYPE4	2.50	0.12552	15.09670	0.15660
8	H12	H10_TYPE3	2.50	0.12552	15.09670	0.12560	8	C3	C04_TYPE4	3.55	0.29288	35.22563	0.09820
9	H14	H0I_TYPE3	2.42	0.12552	15.09670	0.19880	9	C16	C03_TYPE4	3.55	0.31798	38.24497	-0.08180
10	F1	F0S_TYPE3	2.90	0.25104	30.19340	-0.09360	10	C15	C0R_TYPE4	3.55	0.31798	38.24497	0.03670
11	H11	H0Z_TYPE3	2.50	0.12552	15.09670	0.12560	11	H9	H0J_TYPE4	2.50	0.12552	15.09670	0.14230
12	C11	C0U_TYPE3	3.50	0.27614	33.21274	-0.00180	12	C8	C0C_TYPE4	3.55	0.29288	35.22563	0.41510
13	C13	C0Y_TYPE3	3.50	0.27614	33.21274	-0.08850	13	F1	F00_TYPE4	2.90	0.25104	30.19340	-0.15070
14	N2	N0T_TYPE3	3.30	0.71128	85.54796	-0.48730	14	H1	H11_TYPE4	0.00	0.00000	0.00000	0.35730
15	O1	O0K_TYPE3	2.90	0.58576	70.45127	-0.24800	15	C2	C09_TYPE4	3.50	0.33472	40.25787	0.17730
16	C10	C0H_TYPE3	3.50	0.27614	33.21274	-0.01370	16	C17	C12_TYPE4	3.50	0.27614	33.21274	-0.17890
17	C1	C0M_TYPE3	3.55	0.29288	35.22563	0.04220	17	C13	C0K_TYPE4	3.50	0.27614	33.21274	-0.09830
18	H9	H0W_TYPE3	2.50	0.12552	15.09670	0.12560	18	H3	H0O_TYPE4	2.50	0.12552	15.09670	0.12270
19	H17	H1B_TYPE3	2.50	0.12552	15.09670	0.13850	19	H6	H0W_TYPE4	2.50	0.12552	15.09670	0.15620
20	H1	H17_TYPE3	0.00	0.00000	0.00000	0.32570	20	H11	H0G_TYPE4	2.50	0.12552	15.09670	0.14240
21	H6	H12_TYPE3	2.50	0.12552	15.09670	0.14410	21	H4	H0P_TYPE4	2.50	0.12552	15.09670	0.12270
22	C9	C02_TYPE3	3.55	0.29288	35.22563	0.45070	22	C1	C02_TYPE4	3.55	0.29288	35.22563	0.02610
23	H3	H0Q_TYPE3	2.50	0.12552	15.09670	0.12480	23	C12	C0A_TYPE4	3.50	0.27614	33.21274	-0.00950
24	H16	H1A_TYPE3	2.50	0.12552	15.09670	0.13850	24	C6	C0N_TYPE4	3.55	0.31798	38.24497	-0.20670
25	N1	N08_TYPE3	3.25	0.71128	85.54796	-0.44620	25	H14	H06_TYPE4	2.42	0.12552	15.09670	0.21420
26	H15	H0O_TYPE3	2.50	0.12552	15.09670	0.10130	26	H8	H0S_TYPE4	2.50	0.12552	15.09670	0.15660
27	C8	C06_TYPE3	3.55	0.29288	35.22563	0.37840	27	H5	H0V_TYPE4	2.50	0.12552	15.09670	0.15620
28	H13	H07_TYPE3	2.42	0.12552	15.09670	0.19280	28	C5	C07_TYPE4	3.50	0.33472	40.25787	-0.16120
29	H7	H16_TYPE3	2.50	0.12552	15.09670	0.14420	29	C4	C0Q_TYPE4	3.50	0.27614	33.21274	0.09100
30	H5	H13_TYPE3	2.50	0.12552	15.09670	0.14410	30	H2	H0Y_TYPE4	2.50	0.12552	15.09670	0.14040
31	H8	H15_TYPE3	2.50	0.12552	15.09670	0.14420	31	H15	H18_TYPE4	2.50	0.12552	15.09670	0.15520
32	H2	H0F_TYPE3	2.50	0.12552	15.09670	0.13060	32	H13	H10_TYPE4	2.42	0.12552	15.09670	0.18730
33	H19	H00_TYPE3	0.00	0.00000	0.00000	0.39550	33	N2	N05_TYPE4	3.30	0.71128	85.54796	-0.51830
34	C3	C0E_TYPE3	3.55	0.29288	35.22563	0.11800	34	H20	H15_TYPE4	2.50	0.12552	15.09670	0.10530
35	C4	C0C_TYPE3	3.50	0.27614	33.21274	0.07080	35	C11	C0B_TYPE4	3.50	0.27614	33.21274	-0.00970
36	C15	C05_TYPE3	3.55	0.31798	38.24497	0.18460	36	O4	O0M_TYPE4	2.96	0.87864	105.67690	-0.40490
37	C12	C0V_TYPE3	3.50	0.27614	33.21274	-0.00230	37	C7	C01_TYPE4	3.55	0.29288	35.22563	-0.01820
38	C7	C0J_TYPE3	3.55	0.29288	35.22563	0.03730	38	O3	O13_TYPE4	2.96	0.87864	105.67690	-0.65050
39	O2	O01_TYPE3	3.12	0.71128	85.54796	-0.42940	39	H18	H17_TYPE4	2.50	0.12552	15.09670	0.10530
40	C6	C03_TYPE3	3.55	0.31798	38.24497	-0.28440	40	N1	N0E_TYPE4	3.25	0.71128	85.54796	-0.52550
41	H21	H0N_TYPE3	2.50	0.12552	15.09670	0.10130	41	H16	H19_TYPE4	2.50	0.12552	15.09670	0.15520
42	C17	C18_TYPE3	3.50	0.27614	33.21274	-0.15230	42	C14	C0H_TYPE4	3.50	0.27614	33.21274	-0.09420
43	H18	H19_TYPE3	2.50	0.12552	15.09670	0.13850	43	C10	C0D_TYPE4	3.50	0.27614	33.21274	-0.01870
44	C2	C0B_TYPE3	3.50	0.33472	40.25787	0.10590	44	N3	N0U_TYPE4	3.25	0.71128	85.54796	-0.18560
45	O4	O09_TYPE3	2.96	0.87864	105.67690	-0.32070	45	H12	H0F_TYPE4	2.50	0.12552	15.09670	0.14240
46	C16	C0D_TYPE3	3.55	0.31798	38.24497	-0.09110	46	O2	O14_TYPE4	2.96	0.87864	105.67690	-0.65050
47	C5	C0A_TYPE3	3.50	0.33472	40.25787	-0.11050	-	-	-	-	-	-	-

2 Lennard-Jones parameters for host atom (C)

2.1 Lennard-Jones parameters for host disordered carbons

For highly distorted carbon sheets, the value of $\varepsilon_{C\text{-}C}/k_B$ = 36.5 K is somewhat higher than that of the graphite potential ($\varepsilon_{C\text{-}C}/k_B$ = 28 K) due to the effect of curvature[1] (Table S3)). Lennard-Jones potential parameters of disordered carbons are presented in Table S3.

Table S3 Lennard-Jones potential parameters of disordered carbons

Atom name	σ (Å)	ε (kJ/mol)	ε/k_B (K)	Charge (e)
Carbon	3.4	0.3035	36.5	0.0000

2.2 Lennard-Jones parameters for planar graphite

It has been shown that the curvature of carbon surfaces enhances the interaction potential strength of disordered carbon compared to that of planar graphite[2,3]. Lennard-Jones potential parameters of planar graphite are presented in Table S4.

Table S4 Lennard-Jones potential parameters and partial charges of host atom (carbon atoms of graphite for molecular simulations).

Atom name	σ (Å)	ε (kJ/mol)	ε/k_B (K)	Charge (e)
Carbon	3.4	0.2328	28	0.0000

For graphite and single-walled carbon nanotube, the Lennard-Jones parameters are equal to $\sigma_{C\text{-}C}$= 3.4 Å and $\varepsilon_{C\text{-}C}/k_B$=28 K =0.2328 kJ/mol[4–6] (Table S4).

3 Lennard-Jones parameters for counter ions

The presence of different forms of ofloxacin in the simulation box, as described and detailed in the paper, along with the surface charge of the carbon material, necessitates the use of counter ions to maintain charge neutrality. To fulfill this requirement for the MD simulations, we introduced cations (Na^+) and anions (Cl^-) such that the total point charge of each simulation box was zero or very close to zero.

3.1 Lennard-Jones parameters of Na^+

The Lennard-Jones and Coulombic parameters used for Na^+ are summarized in Table S5.

Table S5 Lennard-Jones potential parameters and partial charges of Na^+.

Cation name	σ (Å)	ε (kJ/mol)	ε/k_B (K)	Charge (e)
Na^+	3.33	0.01160	1.39524	+1

The values in Table S5 were taken from https://github.com/paduagroup/fftool/blob/master/examples/oplsaa.ff.

3.2 Lennard-Jones parameters of Cl^-

The Lennard-Jones and Coulombic parameters used for Na^+ are summarized in Table S6.

Table S6 Lennard-Jones potential parameters and partial charges of Cl^-.

Anion name	σ (Å)	ε (kJ/mol)	ε/k_B (K)	Charge (e)
Cl^-	4.417	0.49283	59.27712	-1

The values in Table S6 were taken from https://github.com/paduagroup/fftool/blob/master/examples/oplsaa.ff.

4 Force field parameters of 3-site and 4-site models

4.1 Force field parameters of 3-site models

4.1.1 Force field parameters of water (SPC/E)

The flexible SPC/E, mSPC/Fw, and TIP4P/2005f parameters are presented in this sub-section. The SPC/E and mSPC/Fw are 3-site models, which are computationally efficient for large systems incorporating harmonic and anharmonic bond energies, respectively. The TIP4P/2005f is a 4-site water model that is frequently used in MD simulations with anharmonic bond energy, requiring more computational resources, and simulations involving TIP4P/2005f require longer computation times than those with 3-site water models.

The Lennard-Jones potential parameters and partial charges of SPC/E model[7] are reported in Table S7.

Table S7 Lennard-Jones potential parameters and partial charges of SPC/E[7].

Water (H_2O)		σ (Å)	ε (kJ/mol)	ε/k_B (K)	Charge (e)
Oxygen	O	3.1655	0.6503	78.2131	−0.8476
Hydrogen	H	0	0	0	+0.4238

We note the SPC/E model in the present work is a flexible SPC/E model considering bond (k_i^{bonds}=4331.5300 kJ/mol, r_0=1.0000 Å) and angle (k_i^{angles}=317.5700 kJ/mol and θ_0=109.47°) energies during MD simulations (https://github.com/paduagroup/fftool/blob/master/examples/spce.ff).

4.1.2 Force field parameters of water (TIP3P/Fw)

Table S8 Lennard-Jones potential parameters and partial charges of TIP3P/Fw[8].

Water (H_2O)		σ (Å)	ε (kJ/mol)	ε/k_B (K)	Charge (e)
Oxygen	O	3.1506	0.63680	76.5894	−0.834
Hydrogen	H	0	0	0	+0.417

We note the TIP3P/Fw model in the present work is a flexible TIP3P/Fw model considering bond (k_i^{bonds}=2215.766904 kJ/mol, r_0=0.96 Å) and angle (k_i^{angles}=142.438004 kJ/mol and θ_0=104.5 °) energies during MD simulations ([8]).

4.1.3 Force field parameters of water (OPC3)

Table S9 Lennard-Jones potential parameters and partial charges of OPC3[9].

Water (H_2O)		σ (Å)	ε (kJ/mol)	ε/k_B (K)	Charge (e)
Oxygen	O	3.17427	0.68369	82.2290	−0.8952
Hydrogen	H	0	0	0	+0.4476

We note the OPC3 model in the present work is a flexible OPC3 model considering bond (k_i^{bonds}=4331.53 kJ/mol, r_0=0.9789 Å) and angle (k_i^{angles}=317.57 kJ/mol and θ_0=109.47°) energies during MD simulations (https://github.com/paduagroup/fftool/blob/master/examples/opc3.ff).

4.1.4 Force field parameters of water (mSPC/Fw)

The Lennard-Jones potential parameters and partial charges of mSPC/Fw model[10] are reported in Table S10.

Table S10 Lennard-Jones potential parameters and partial charges of mSPC/Fw model[10]

Water (H_2O)		σ (Å)	ε (kJ/mol)	ε/k_B (K)	Charge (e)
Oxygen	O	3.554	0.650299	78.2497	−0.82
Hydrogen	H	0	0	0	+0.41

In the mSPC/Fw model unlike SPC/E model, the bond energy is anharmonic and can be denoted by Morse potential ($U_{bond}(r) = \sum_{bonds} D0_i^{bond}\left[\exp\left(-2\alpha_i^{bonds}(r-r_0)\right) - 2\exp\left(-\alpha_i^{bonds}(r-r_0)\right)\right]$). The bond energy parameters are $D0_i^{bond}$=492.2681 kJ/mol, α_i^{bonds}=2.1578 1/Å, r_0=1.012 Å. The angle energy is harmonic like SPC/E ($U_{angle}(r) = \sum_{angles} k_i^{angles}(\theta_i - \theta_0)^2$). The parameters of angle energy are k_i^{angles}=424.1496 kJ/mol/rad^2 and θ_0=113.24°.

4.2 Force field parameters of 4-site models

4.2.1 Force field parameters of water (OPC)

Table S11 Lennard-Jones potential parameters and partial charges of OPC[11].

Water (H_2O)		σ (Å)	ε (kJ/mol)	ε/k_B (K)	Charge (e)
Oxygen	O†	3.16655	0.89036	107.0857	−1.3582
Hydrogen	H	0	0	0	+0.6791

†Point charge of oxygen atom is shifted to fictive atom at 0.1594 Å.

We note the OPC model in the present work is a flexible OPC model considering bond (k_i^{bonds}=4331.53 kJ/mol, r_0=0.8724 Å) and angle (k_i^{angles}=317.57 kJ/mol and θ_0=103.6 °) energies during MD simulations (https://github.com/paduagroup/fftool/blob/master/examples/opc.ff).

Table S12 Lennard-Jones potential parameters and partial charges of TIP4P[12].

Water (H_2O)		σ (Å)	ε (kJ/mol)	ε/k_B (K)	Charge (e)
Oxygen	O†	3.1536	0.64852	77.9990	−1.04
Hydrogen	H	0	0	0	+0.52

†Point charge of oxygen atom is shifted to fictive atom at 0.15 Å.

4.2.2 Force field parameters of water (TIP4P)

We note the TIP4P model in the present work is a flexible TIP4P model considering bond (k_i^{bonds}=4331.53 kJ/mol, r_0=0.9572 Å) and angle (k_i^{angles}=317.57 kJ/mol and θ_0=104.52 °) energies during MD simulations (https://github.com/paduagroup/fftool/blob/master/examples/tip4p.ff).

4.2.3 Force field parameters of water (TIP4P-Ew)

Table S13 Lennard-Jones potential parameters and partial charges of TIP4P-Ew[13].

Water (H_2O)		σ (Å)	ε (kJ/mol)	ε/k_B (K)	Charge (e)
Oxygen	O†	3.16435	0.680946	81.8989	−1.04844
Hydrogen	H	0	0	0	+0.52422

†Point charge of oxygen atom is shifted to fictive atom at 0.1594 Å.

We note the TIP4P-Ew model in the present work is a flexible TIP4P-Ew model considering bond (k_i^{bonds}=4331.53 kJ/mol, r_0=0.9572 Å) and angle (k_i^{angles}=317.57 kJ/mol and θ_0=104.52 °) energies during MD simulations (https://github.com/paduagroup/fftool/blob/master/examples/tip4pew.ff).

4.2.4 Force field parameters of water (TIP4P/2005f)

The Lennard-Jones potential parameters and partial charges of TIP4P/2005f[14] are reported in Table S14.

Table S14 Lennard-Jones potential parameters and partial charges of TIP4P/2005f[14]

Water (H_2O)		σ (Å)	ε (kJ/mol)	ε/k_B (K)	Charge (e)
Oxygen	O†	3.1644	0.774906	93.2436	−1.1128
Hydrogen	H	0	0	0	+0.5564

†Point charge of oxygen atom is shifted to fictive atom at 0.15555 Å.

The TIP4P/2005f water model, like mSPC/Fw, is flexible and also exhibits anharmonic stretching at the OH bond (Morse potential). We account for the bond energy ($D0_i^{bonds}$ = 432.5809 kJ/mol, α_i^{bonds} = 2.287 1/Å, r_0 = 0.9419 Å, and O − M = 0.15555 Å) and angle energy (k_i^{angles} = 367.810 kJ/mol/rad^2, θ_0 = 107.4°, and ϕ_0 = 53.7°) during the MD simulations.

5 Unraveling the Most Promising Water Model: Structural and Dynamic Properties and Gibbs free energy of solvation

5.1 Structural Properties

The most important structural properties of water molecules include the density and coordination numbers, particularly at the peak positions of the Ow-Ow, Ow-Hw, and Hw-Hw RDFs.

All water models are generally parameterized to reproduce the structural properties of water, as discussed above. A comparison of the models described in Supplementary materials 4 is presented in Figures S1 to S3. In Figure S1, the RDFs of Ow-Ow and Ow-Hw for all selected water models are compared with experimental data. As expected, the models generally align well with experiments since they are designed to do so. To better visualize the differences between experimental data and our MD simulations, the RDF peak positions are shown in radar charts in Figure S2. The most significant discrepancies occur at the first peaks of the Ow-Ow and Hw-Hw distributions.

The second RDF peak is also important and can be compared to experiments. We evaluated it using our MD simulations and calculated the coordination number with PyLAT[15].

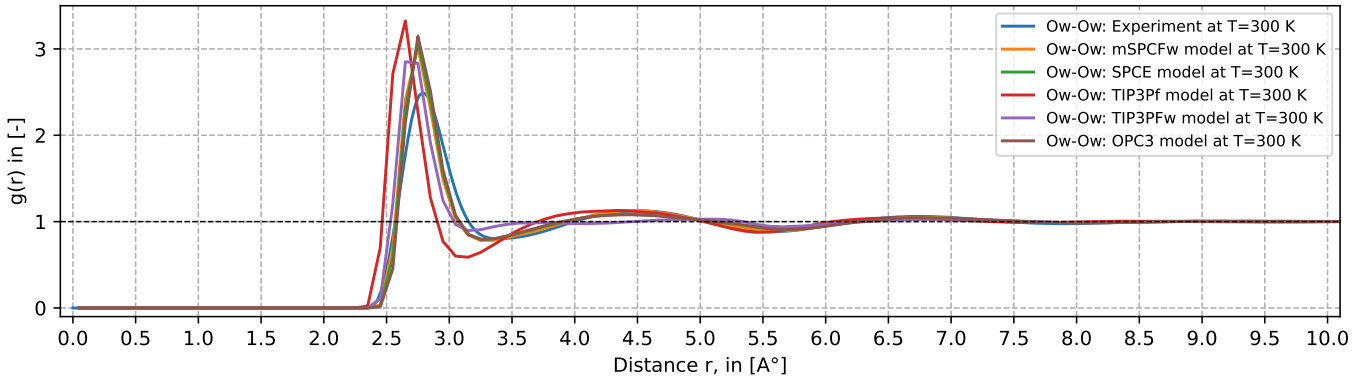

(a) Ow-Ow RDF of 3-site models

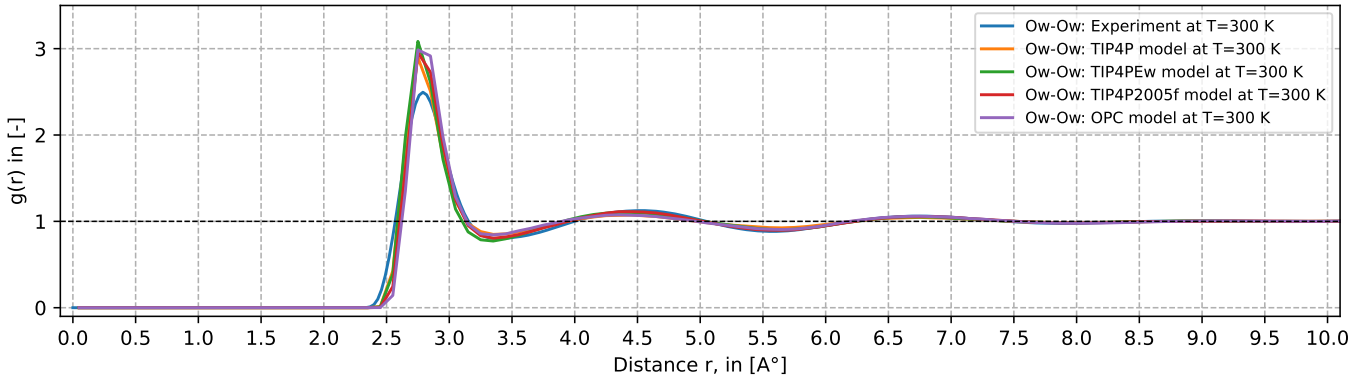

(b) Ow-Ow RDF of 4-site models

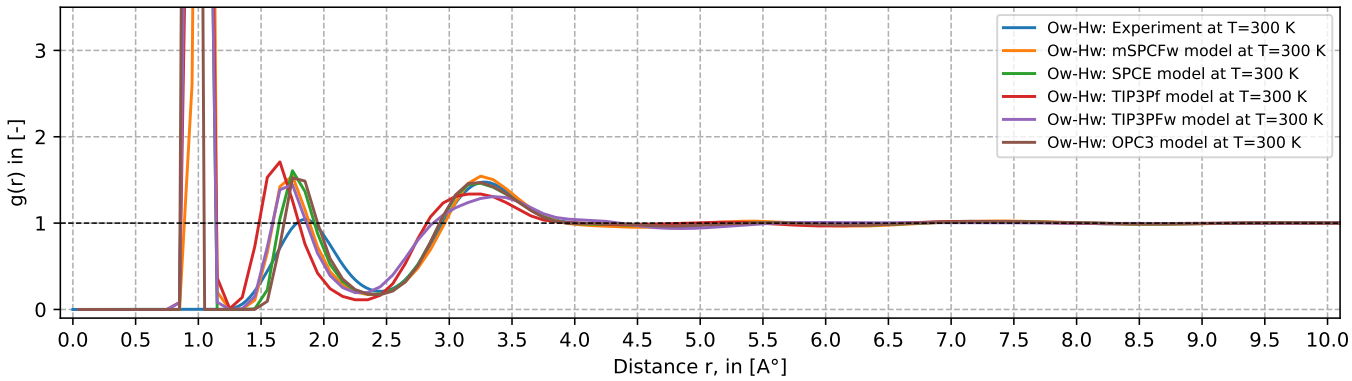

(c) Ow-Hw RDF of 3-site models

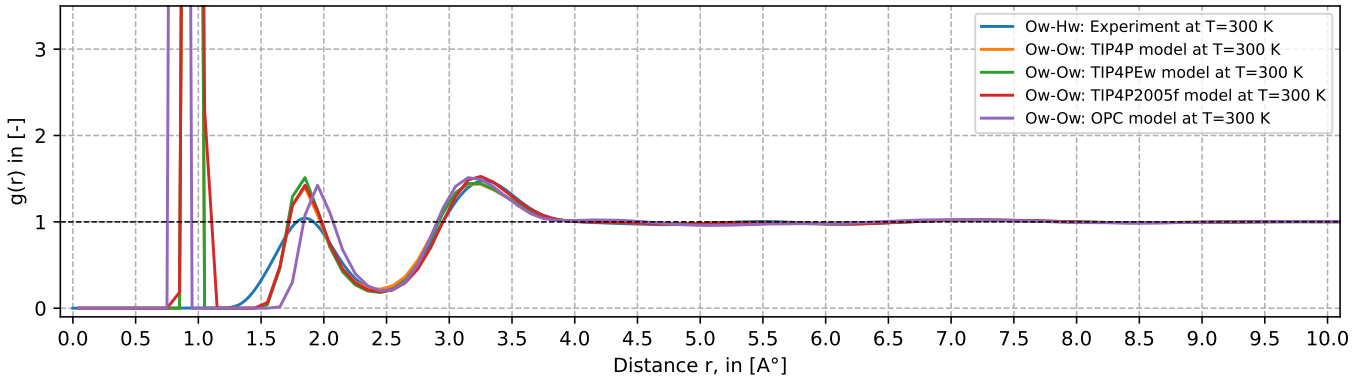

(d) Ow-Hw RDF of 4-site models

Fig. S1 RDF graphs for Ow-Ow and Ow-Hw interactions in frequently used 3-site and 4-site water models.

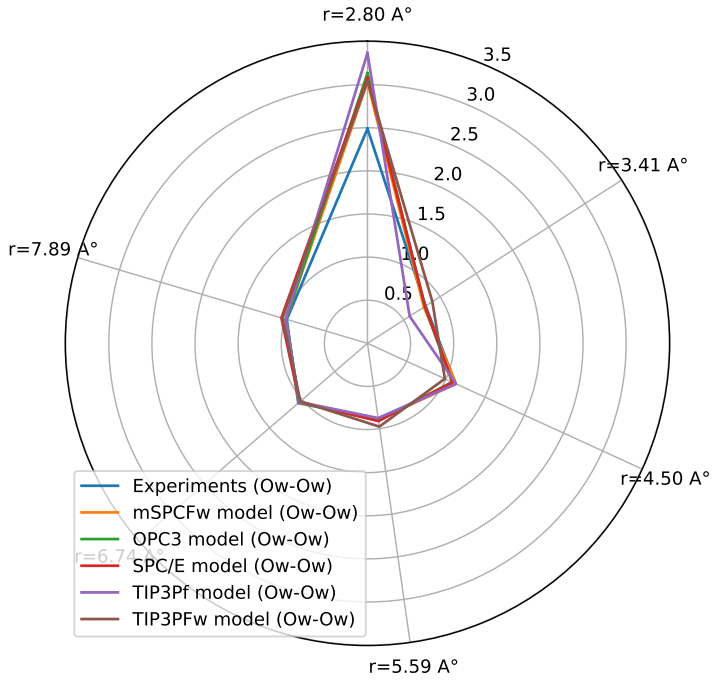

(a) Peaks of Ow-Ow RDF for 3-site water models

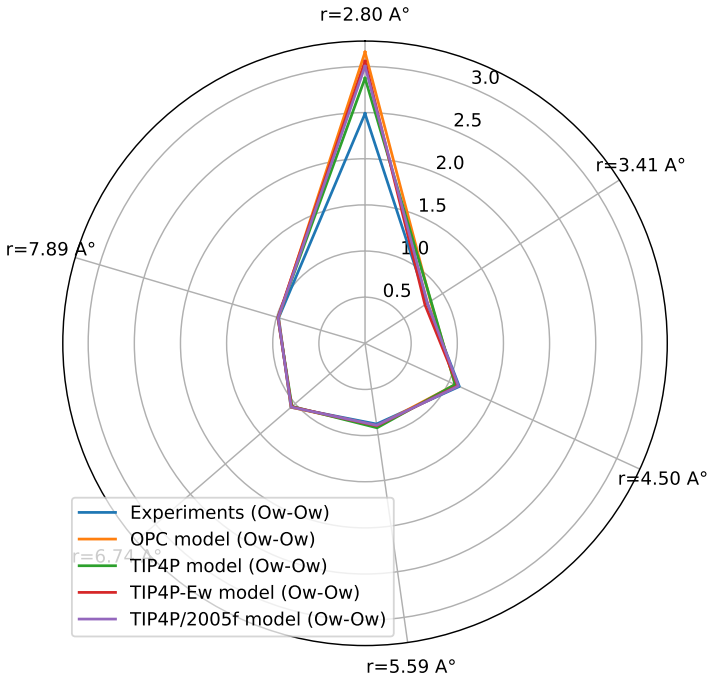

(b) Peaks of Ow-Ow RDF for 4-site water models

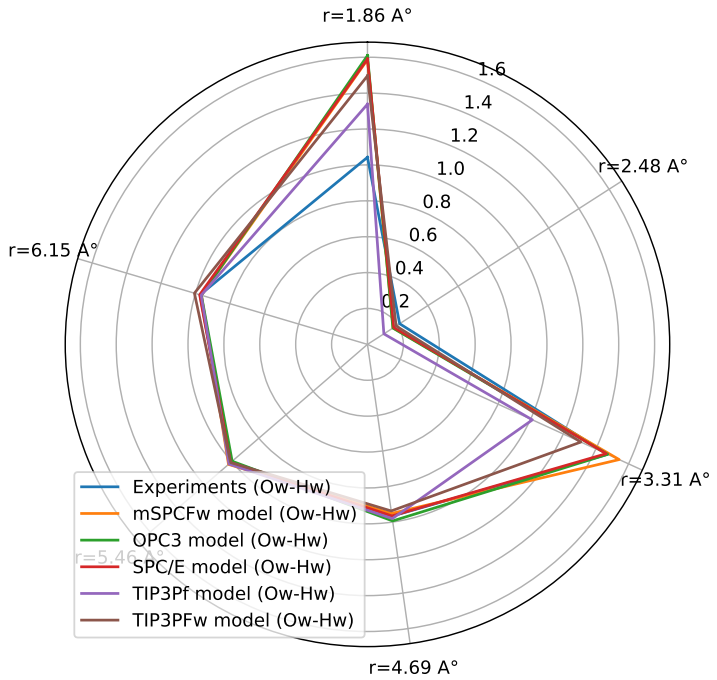

(c) Peaks of Ow-Hw RDF for 3-site water models

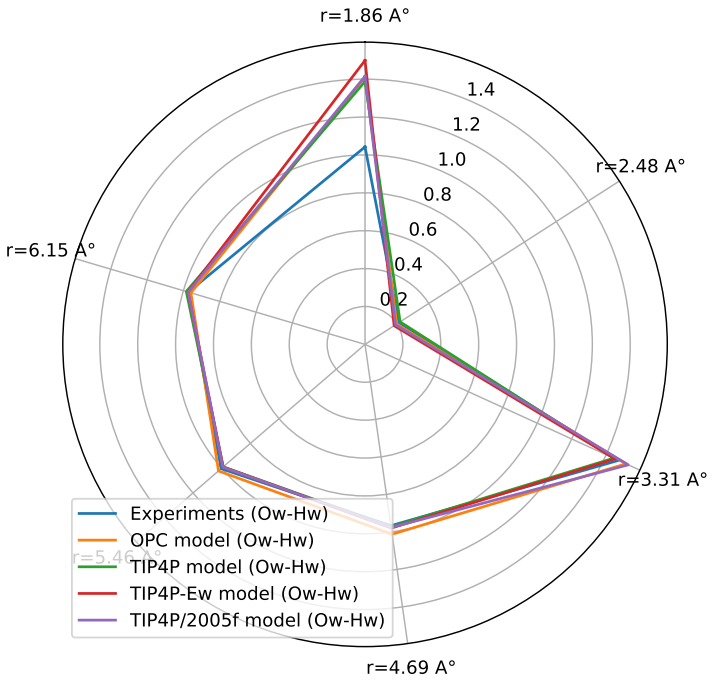

(d) Peaks of Ow-Hw RDF for 4-site water models

Fig. S2 Radar charts comparing Ow-Ow and Ow-Hw RDF peak positions of frequently used 3-site and 4-site water models with experimental data.

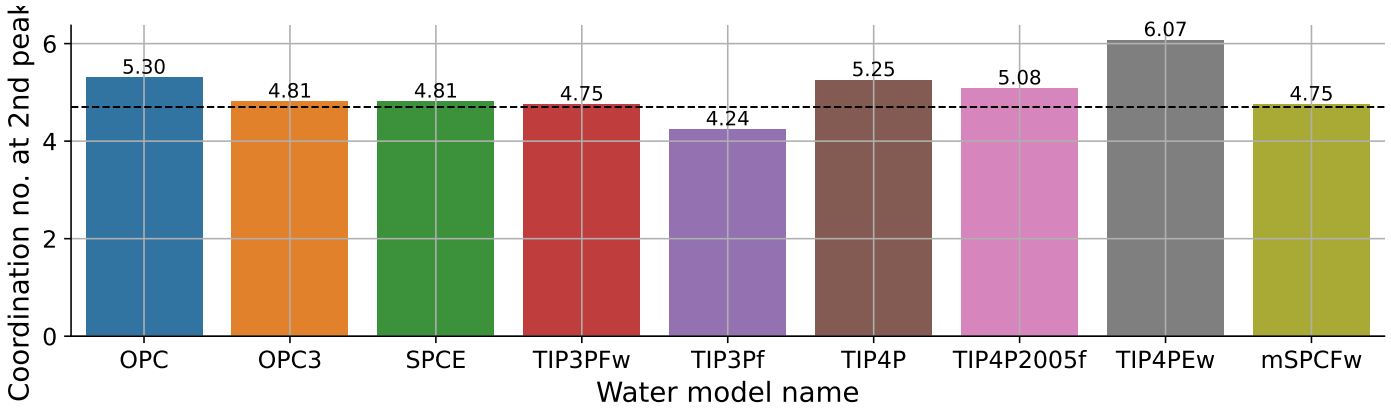

Fig. S3 Coordination number at the second peak of the Ow-Ow RDF for different water models[16].

As shown in Figures S1 to S3, most of the 3-site and 4-site models successfully reproduce the expected structural features of water. Among them, SPC/E, mSPC/Fw, and TIP4P/2005f stand out as particularly reliable choices for capturing structural properties.

5.2 Dynamic Properties of Water Models

The self-diffusion coefficient, dielectric constant, and vibrational spectra represent three key dynamic properties of water models, as shown in Figures S4 and S5 and Figures S6 and S8.

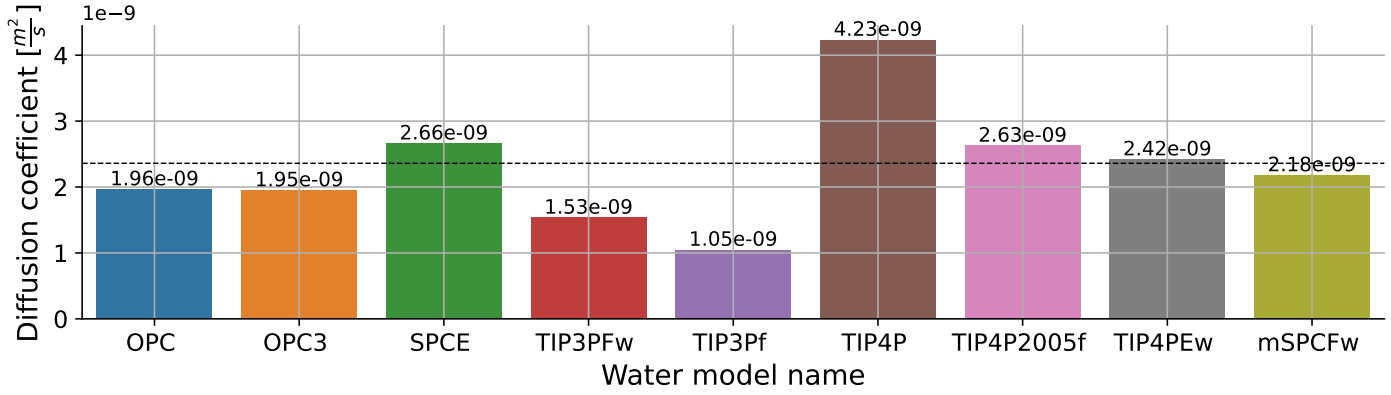

Fig. S4 Self-diffusion coefficient of water models.

The diffusion coefficient was computed using user-written TCL script for VMD[17], while the dielectric constant was determined via PyLAT[15]. The vibrational spectra were obtained by calculating the auto-correlation of molecular dynamics (MD) trajectory data using a VMD plugin. As shown in Figures S4 and S5, the SPC/E, mSPC/Fw, and TIP4P/2005f models again exhibit good agreement with experimental data, making them strong candidates for reliable water modeling in this study.

For the vibrational spectra, we conducted both density functional theory (DFT) calculations using the B3LYP exchange functional and the TZ2P basis set via ADF[18], and MD simulations using the LAMMPS package[19]. These results were compared with experimental data reported in the literature[20].

Among the studied models, the SPC/E model shows significant deviations in vibrational spectra compared to mSPC/Fw and TIP4P/2005f, as illustrated in Figures S6 and S8. For DFT simulations, we note that H-O-H bending mode is accurately reproduced by the selected exchange functional and basis set, whereas the O-H stretching mode is not well captured by DFT. This limitation arises because DFT does not fully account for intermolecular interaction in driven spectral intensities, an aspect that is better addressed by MD simulations. MD simulations, on the other hand, capture both intermolecular and intramolecular vibrational features, as demonstrated in Figures S6 and S8. Among all tested 3-site and 4-site models, only mSPC/Fw and TIP4P/2005f successfully reproduce the complete vibrational spectra, especially in the region around 3400 cm^{-1}, as highlighted in Figures S6d and S7d. Based on further analysis[21], TIP4P/2005f appears to be the most appropriate model for accurately capturing both structural and dynamic properties of water. Therefore, it is employed for all MD simulations throughout this work.

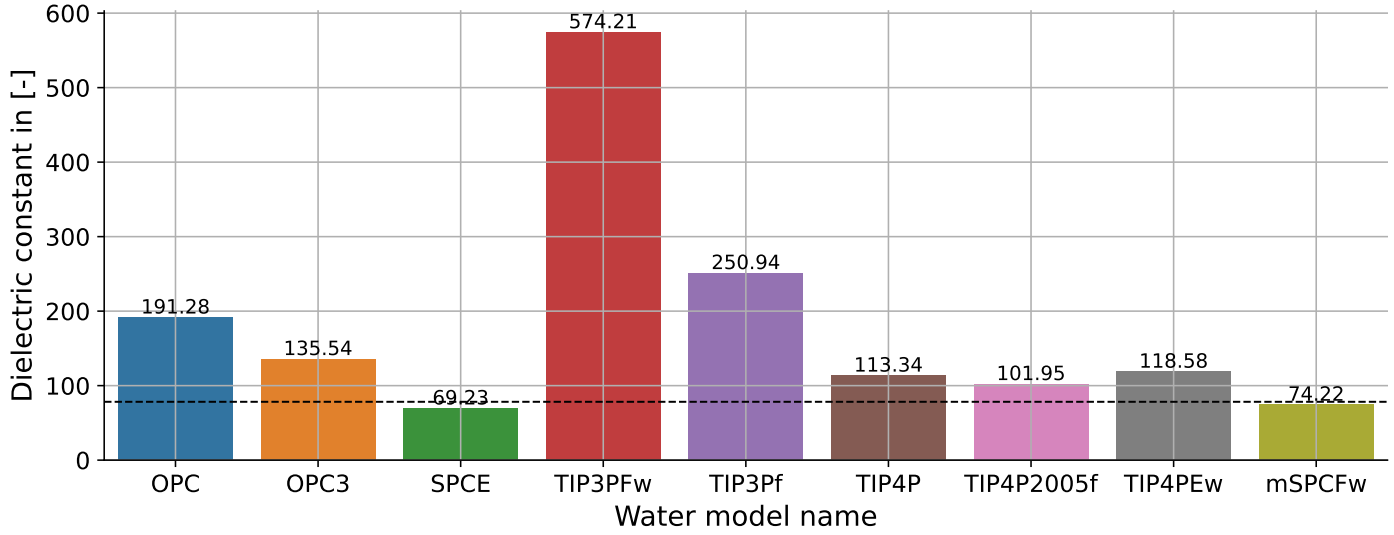

Fig. S5 Dynamic properties of different water models computed via MD simulations[16].

6 Gibbs free energy of solvation

Solvation is the physicochemical process of dissolution in which a chemical substance (the solute) becomes surrounded by solvent molecules. This phenomenon is characterized by a change in Gibbs free energy (ΔG_{solv}) at constant temperature and pressure[22]. The solvation of an organic molecule is strongly influenced by its specific physicochemical properties, such as polarity, hydrogen bonding, and microscopic structure, as well as those of the solvent itself. Consequently, it is essential to identify a water model capable of accurately reproducing solvation energies that closely align with experimental measurements. Various numerical methods can be employed to calculate this thermodynamic quantity, including Molecular Dynamics (MD), Monte Carlo (MC), or Density Functional Theory (DFT) simulations. In MD, a perturbation is applied to the interaction potential parameters to recalculate the pair potential energy without altering the atomic coordinates relative to the unperturbed reference system.

This can be achieved using Free-Energy Perturbation (FEP), Finite-Difference Thermodynamic Integration (FDTI), or Bennett's Acceptance Ratio (BAR) method[23]. In this work, we utilized the FEP method, as implemented in the LAMMPS software package[19,24] as shown in Figure S8. The comparison among water models shows, once again, that the flexible anharmonic TIP4P/2005f water model produces methane molecule insertion and withdrawal energy values that are close to the experimental results (2 kcal/mol or 8.368 kJ/mol), along with the SPC/E model.

These two well-established methods (Free Energy Perturbation (FEP) and Finite-Difference Thermodynamic Integration (FDTI)) were employed to compute the solvation free energy via insertion and withdrawal of a methane molecule in water, serving as a standard validation test for the selected water model. However, a significant limitation arises for the ofloxacin system, since these methods are not readily applicable to ionic species, making rigorous evaluation of water-ofloxacin interactions considerably more challenging

7 Elemental analysis and atomic percentage of KIP1200

The elemental analysis and atomic percentage of KIP1200 are shown in Figure S9.

8 HRMC flowchart and 2-stage modeling concept

The procedure begins with MC relaxation, in which the simulated RDF and SF, are computed alongside its total energy and any other relevant constraints. The experimental and simulated data are then compared using the cost function defined in Equations (9a) and (9b):

$$\chi_{total,old} = \sum_i \sum_j \frac{\left(A_{ij}^{exp} - A_{ij}^{sim,old}\right)^2}{W_i} + \frac{E^{old}}{k_B T} \tag{9a}$$

$$\chi_{total,new} = \sum_i \sum_j \frac{\left(A_{ij}^{exp} - A_{ij}^{sim,new}\right)^2}{W_i} + \frac{E^{new}}{k_B T} \tag{9b}$$

Here, the first term represents the weighted difference between the experimental (target) value of A_{ij}^{exp} and the previous simulation value $A_{ij}^{sim,old}$, scaled by the weighting factor W_i, while the second term is the system's total energy E^{old} normalized by the product of

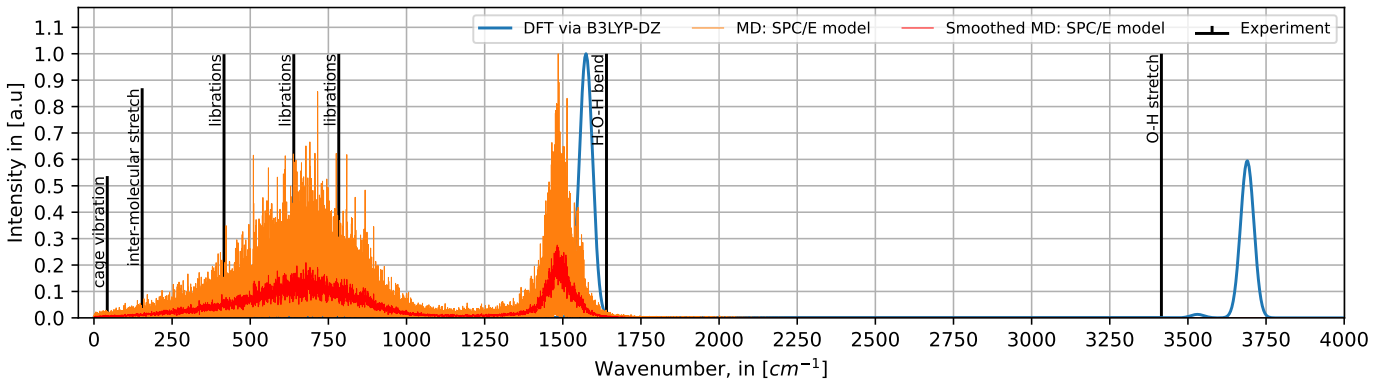

(a) SPC/E model

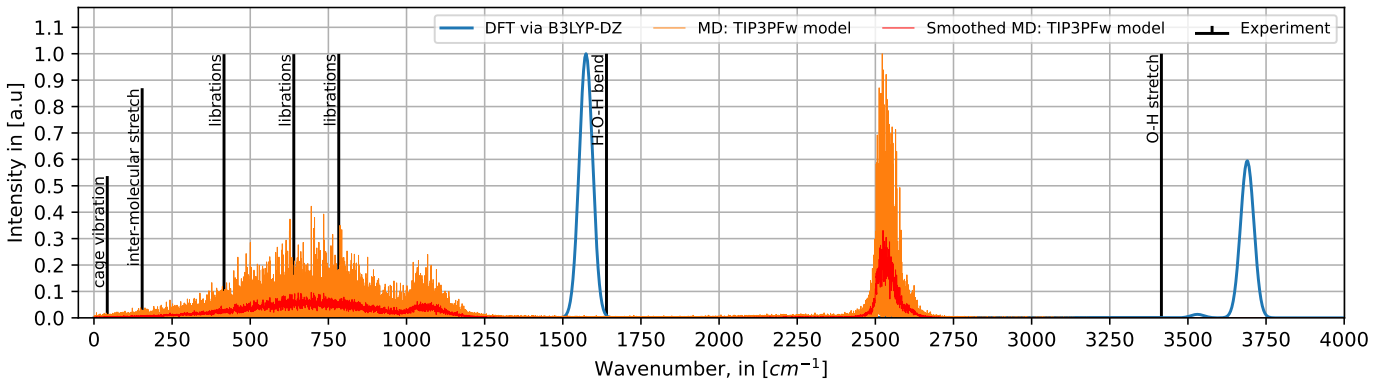

(b) TIP3P/Fw model

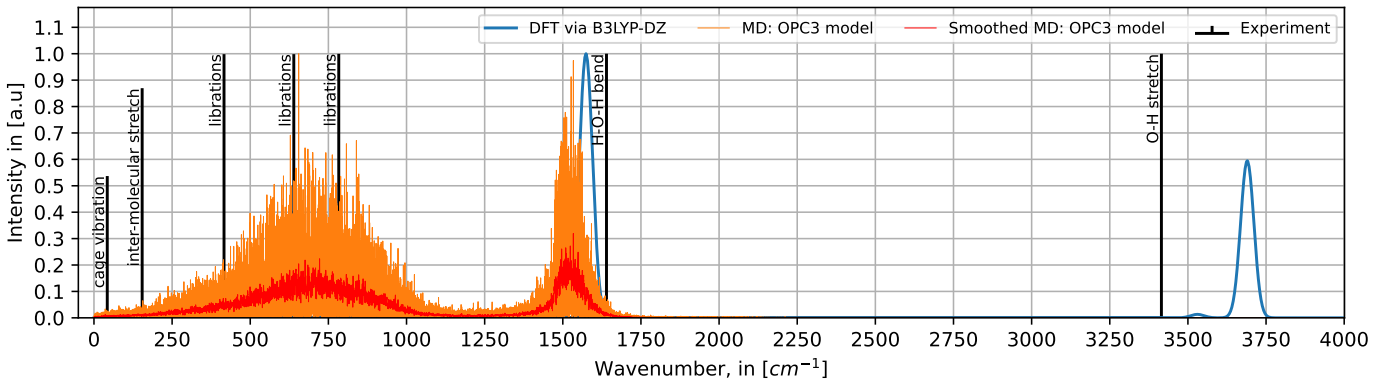

(c) OPC3 model

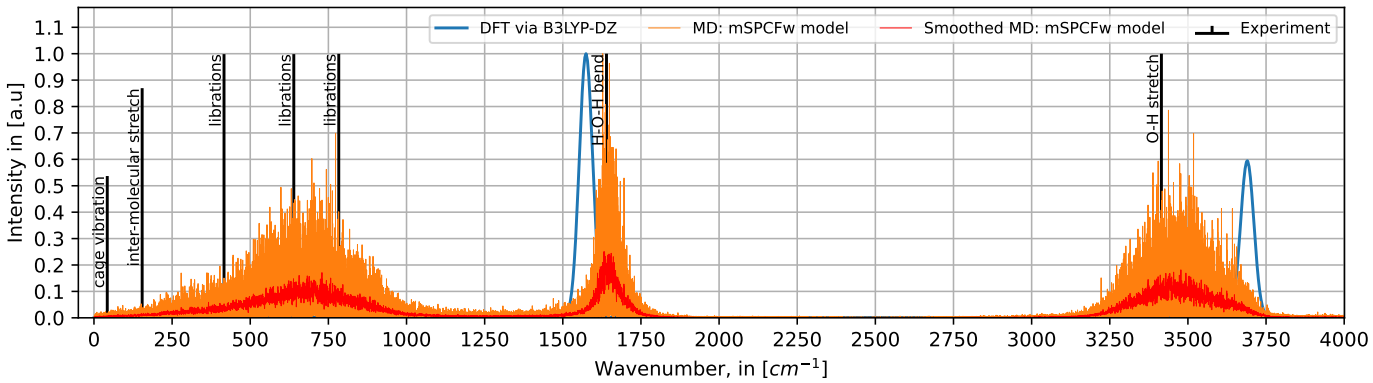

(d) mSPC/Fw model

Fig. S6 MD vibrational spectra of 3-site water models compared to DFT and experimental results.

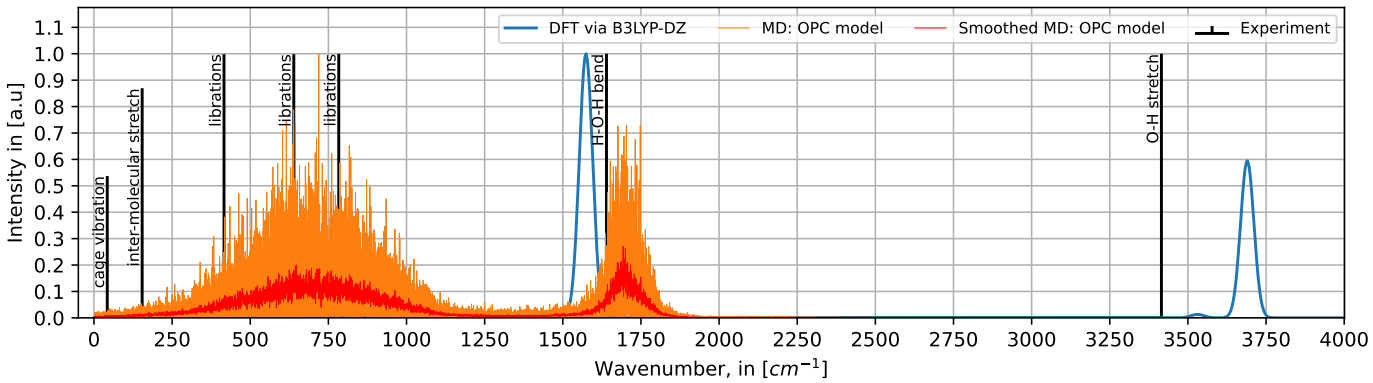

(a) OPC model

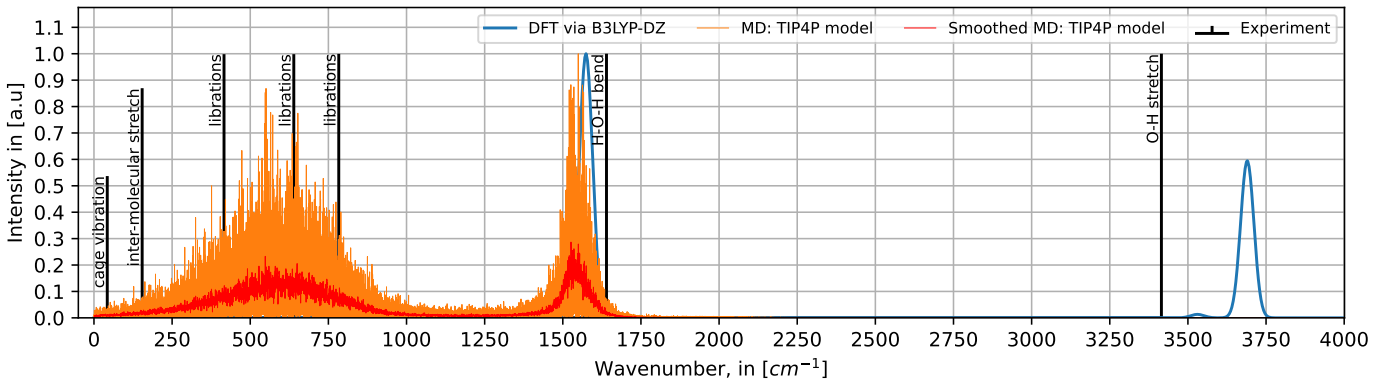

(b) TIP4P model

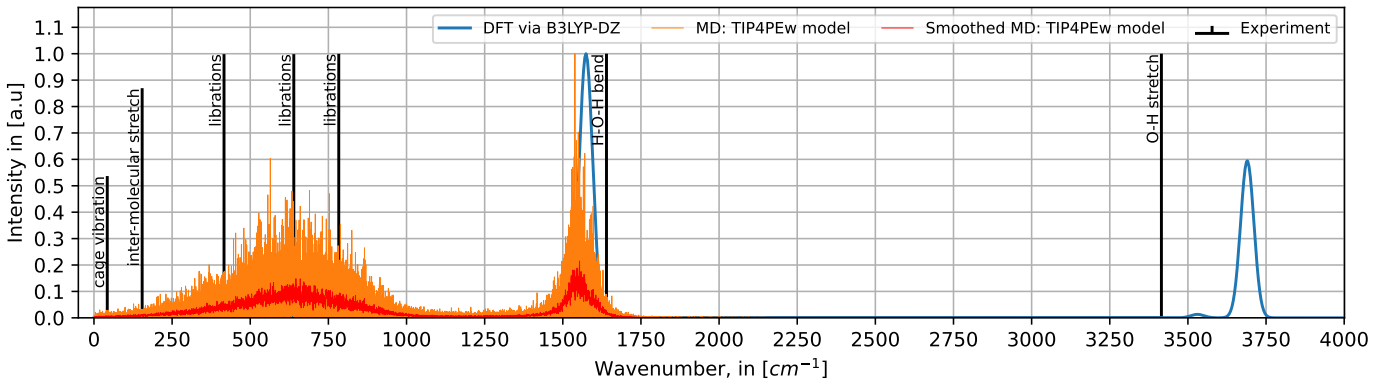

(c) TIP4P-Ew model

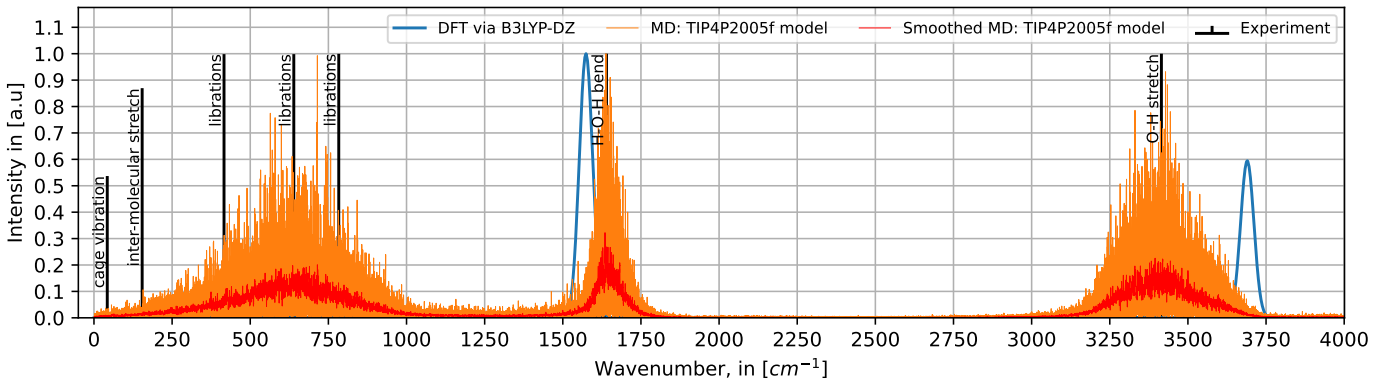

(d) TIP4P/2005f model

Fig. Journal Name, [year], **[vol.]**, 1–20 4-site water models compared to DFT and experimental results.

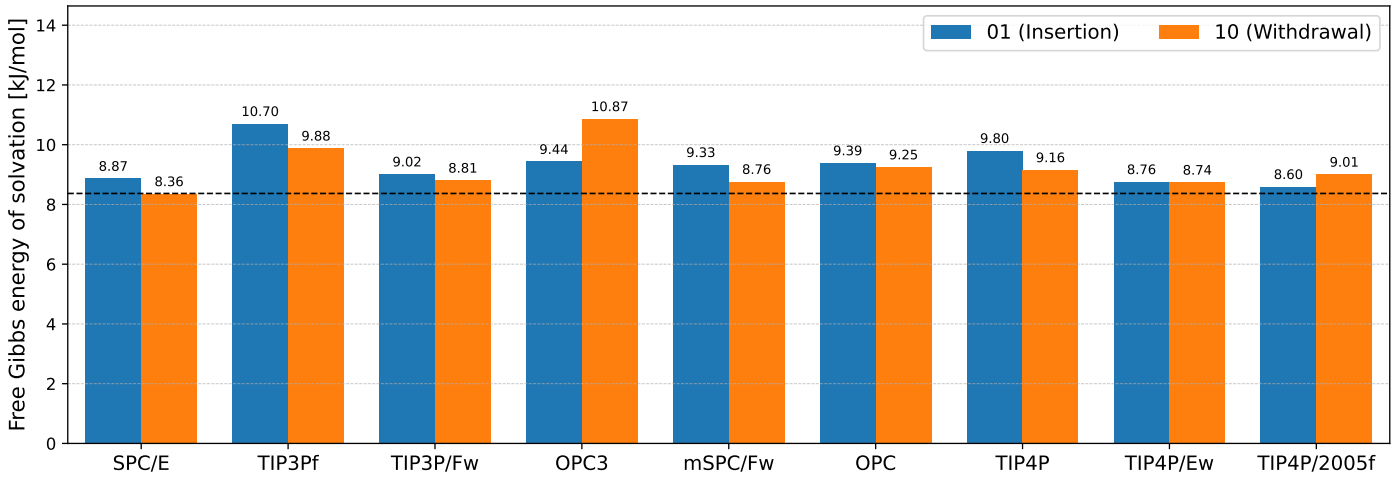

Fig. S8 Solvation free energy of methane obtained for each water model using the FEP method. Blue histograms represent the insertion energies, while orange histograms represent the deletion energies.

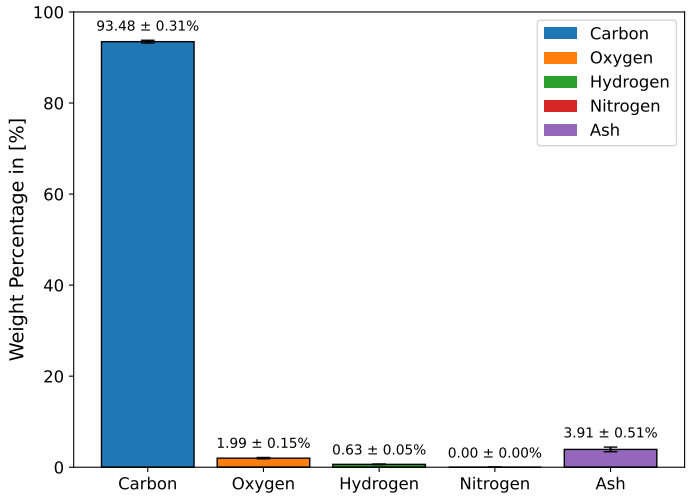

(a) Weight percent

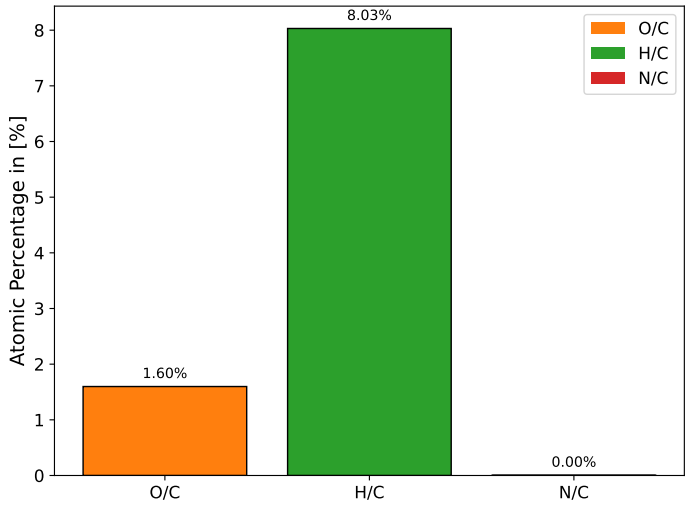

(b) Atomic percent

Fig. S9 (a) Elemental composition of KIP1200 in weight percent by a CHNO Analyzer, and (b) Atomic percentage[25].

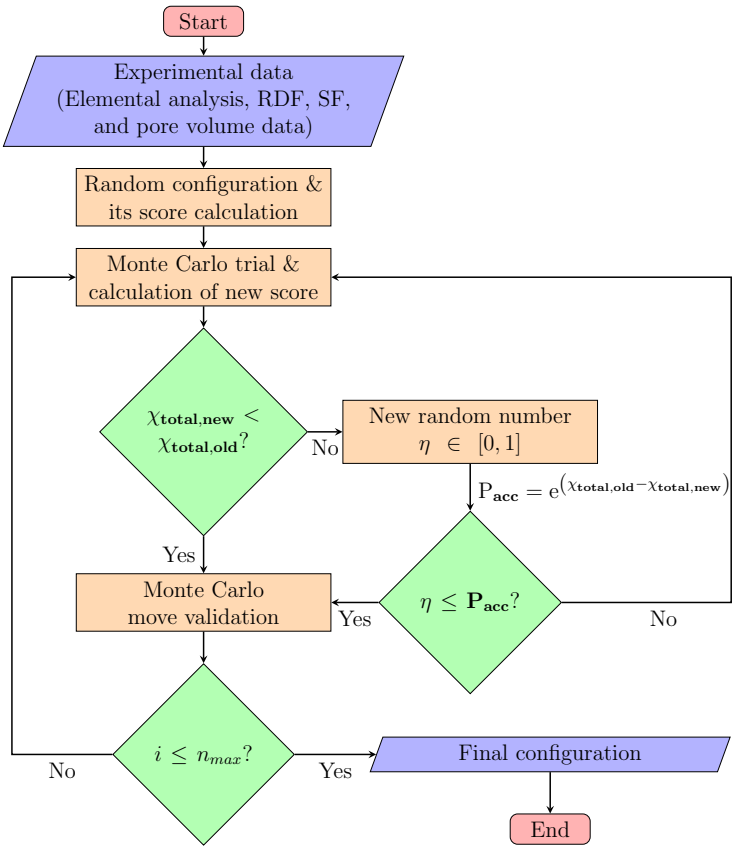

Fig. S10 HRMC modeling flowchart.

the Boltzmann constant k_B and the temperature T (Figure S10). Next, there is a trial Monte Carlo moves to minimize the total error and the calculation of a new function cost (Equation (9b)) which is compared to the old one. The new configuration is accepted only if and only $\chi_{\text{total,new}} < \chi_{\text{total,old}}$ or $\eta < P_{acc}$, where η a random variable on $[0,1]$ and $P_{acc} = \exp\left(\chi_{\text{total,old}} - \chi_{\text{total,new}}\right)$ the probability of acceptance. This procedure is repeated until convergence is achieved.

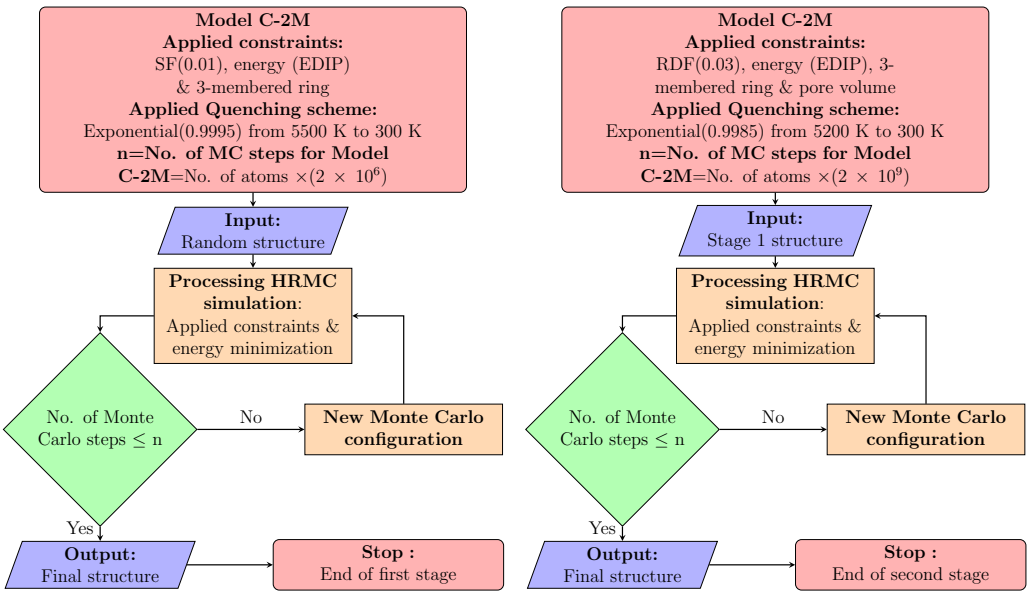

(a) HRMC modeling: Stage 1 **(b)** HRMC modeling: Stage 2

Fig. S11 HRMC modeling procedures using 2-stage modeling.

The modeling scheme is illustration in Figure S11 highlighting stage 1 (Figure S11a) and stage 2 (Figure S11b).

9 Fugacity Calculation of N_2 and CO_2 for GCMC Simulations

9.1 Basic Equation for the Fugacity of Pure Gases

The fugacity of pure gases, such as N_2 and CO_2, can be approximated using Equation (10), as reported by Weiss[26]:

$$\ln\left(\frac{F}{P}\right) = \frac{B(T) \times P}{RT} \Rightarrow F = P\exp\left(\frac{B(T) \times P}{RT}\right) \tag{10}$$

Here, F, P, B(T), R, and T represent the fugacity, pressure, second virial coefficient of the gas, universal gas constant, and temperature (in K), respectively. The fugacity coefficient can then be calculated from the fugacity and pressure[27,28], as shown in Equation (11):

$$f = \frac{F}{P} \tag{11}$$

The most challenging aspect of calculating fugacity lies in the accurate determination of the second virial coefficient, B(T), as a function of temperature. Dymond et al. provided recommended values and equations that allow for accurate computation of fugacity over a range of pressures and temperatures[29].

9.2 Second Virial Coefficient of N_2 and CO_2

9.2.1 Second Virial Coefficient of N_2

For N_2, we used the temperature-dependent expression for the second virial coefficient provided by Dymond et al.[29], as shown in Equation (12):

$$B(T) = 4.0286 \times 10 - \frac{9.3378 \times 10^3}{T} - \frac{1.4164 \times 10^6}{T^2} + \frac{6.1253 \times 10^7}{T^3} - \frac{2.7198 \times 10^9}{T^4} \tag{12}$$

where B(T) is expressed in cm^3/mol, and T is the temperature in K.

9.2.2 Second Virial Coefficient of CO_2

For CO_2, we employed the polynomial expression proposed by Sanders et al.[30] and utilized elsewhere[26], which is valid in the temperature range of 265-320 K, as shown in Equation (13):

$$B(T) = -1636.75 + 12.0408 \times T - 3.27957 \times 10^{-2} \times T^2 + 3.16528 \times 10^{-5} \times T^3 \tag{13}$$

Here, B(T) is given in cm^3/mol, and T is the temperature in K.

10 Isotherm model

10.1 Langmuir model

This models assumes that adsorption must be single-layered with one molecule per site at equilibrium and where the speed of a molecule to adsorb is equal to the speed to desorb[31]. It is assumed that all sites are equivalent and there are no lateral interactions between the adsorbed molecules[32–34]. This model is characterized by two fitting parameters: Q_e and Q_m.

$$Q_e = \frac{Q_m K_L C_e}{1 + K_L C_e} \tag{14}$$

where Q_e represents the adsorption capacity (mmol/g), Q_m is the maximum adsorption capacity (mmol/g), and K_L is the Langmuir constant (L/mmol). The most important parameter of the Langmuir isotherm is its phase separation factor R_L, expressed as:

$$R_L = \frac{1}{1 + K_L C_0} \quad ; \text{where } C_0 \text{ is initial concentration of ofloxacin solution} \tag{15}$$

where the value of R_L indicates whether the isotherm is reversible ($R_L = 0$), favorable ($0 < R_L < 1$), linear ($R_L = 1$) or unfavorable ($R_L > 1$).

10.2 Freundlich model

The Freundlich model[35], proposed by Freundlich in 1907, describes adsorption processes occurring on heterogeneous surfaces, with Q_e representing the adsorption capacity. It is expressed by the following equation:

$$Q_e = K_F \times C_e^{\frac{1}{n_F}} \tag{16}$$

where Q_e is the adsorbed quantity, C_e is the equilibrium concentration, K_F is the Freundlich adsorption capacity coefficient, and n is the Freundlich exponent. The Freundlich isotherm assumes that molecules are distributed on the surface according to Boltzmann's law, and the adsorption energies are much higher than thermal energy[32], so it applies to surfaces with heterogeneous energy.

10.3 Langmuir-Freundlich model

The Langmuir-Freundlich isotherm takes into account adsorption on heterogeneous surfaces[36]. It describes the distribution of adsorption energy on the heterogeneous surface of the adsorbent[37]. At low adsorbate concentration, this model becomes the isothermal Freundlich model, while at high adsorbate concentration it becomes the Langmuir isotherm[37]. It is expressed as follows:

$$Q_e = \frac{Q_m (K_{LF} C_e)^{\frac{1}{n_{LF}}}}{1 + (K_{LF} C_e)^{\frac{1}{n_{LF}}}} \tag{17}$$

where Q_m is the maximum adsorption capacity (mmol/g), K_{LF} is the equilibrium constant for heterogeneous solids, and 1/n is the heterogeneity parameter, ranging between 0 and 1.

11 Ofloxacin adsorption kinetics on activated carbon (KIP1200)

The ofloxacin adsorption kinetic are shown in Figure S12 for different solution pH.

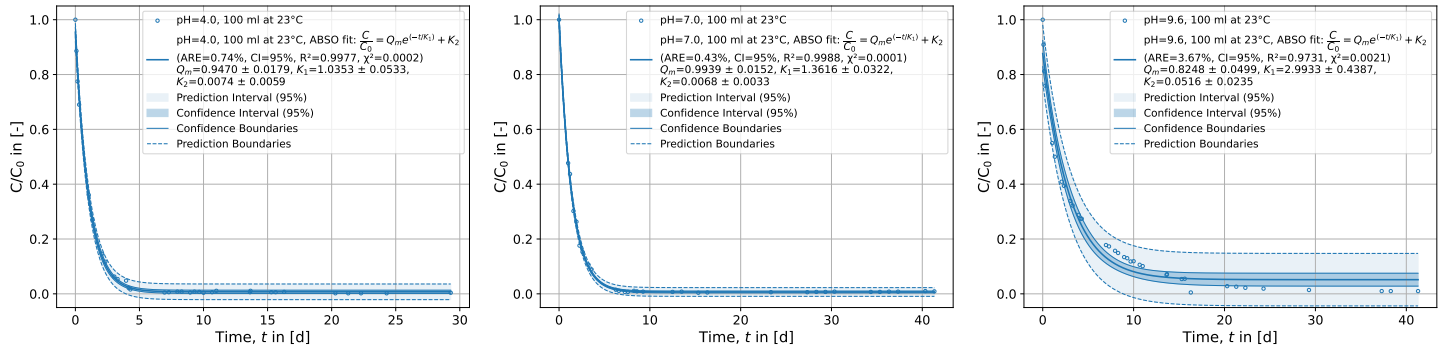

(a) pH=4.0 **(b)** pH=7.0 **(c)** pH=9.6

Fig. S12 Ofloxacin adsorption kinetics on activated carbon (KIP1200) a) pH=4.0, b) pH=7.0, and c) pH=9.6 at 23 °C.

12 Ofloxacin isotherm graphs: Langmuir model with confidence interval

The Langmuir model with confidence interval of 95% and prediction boundaries is shown in Figure S13 for pH=4.0, 7.0 and 9.6.

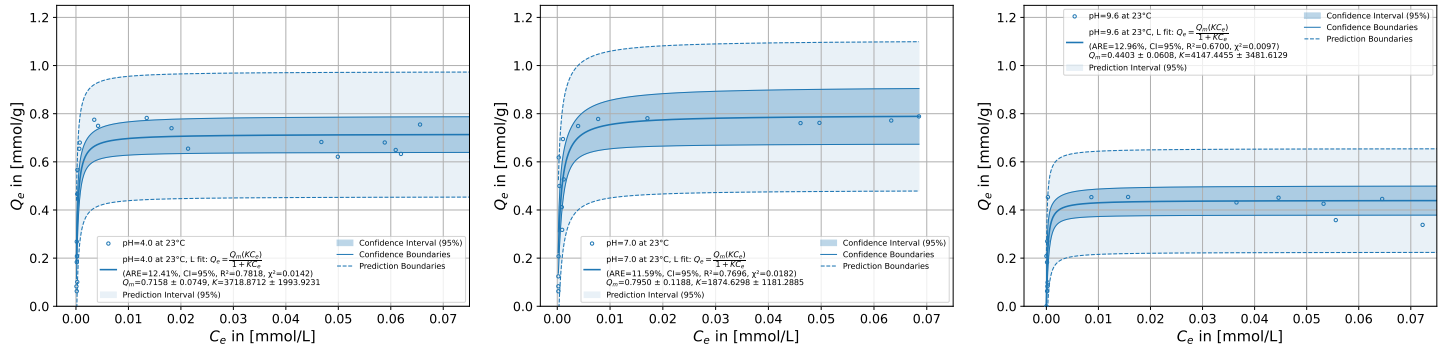

(a) pH=4.0 **(b)** pH=7.0 **(c)** pH=9.6

Fig. S13 Langmuir adsorption isotherms for (a) pH=4.0, (b) 7.0, and (c) 9.6 at 23°C.

13 Ofloxacin isotherm graphs: Freundlich and Langmuir-Freundlich models

Here, we present the results of Freundlich[35] and Langmuir-Freundlich[36] isotherm models for the ofloxacin solution at different pH values: 4.0, 7.0, and 9.6.

13.1 Results of Freundlich model for ofloxacin

In Figure S14, the Freundlich isotherm models are plotted with a 95% confidence interval, including the confidence and prediction boundaries. We can observe the poor statistical fit of the Freundlich method as shown in Figures S14a to S14c. Overall, the Freundlich model is not a good choice for modeling the ofloxacin adsorption isotherms compared to the Langmuir model.

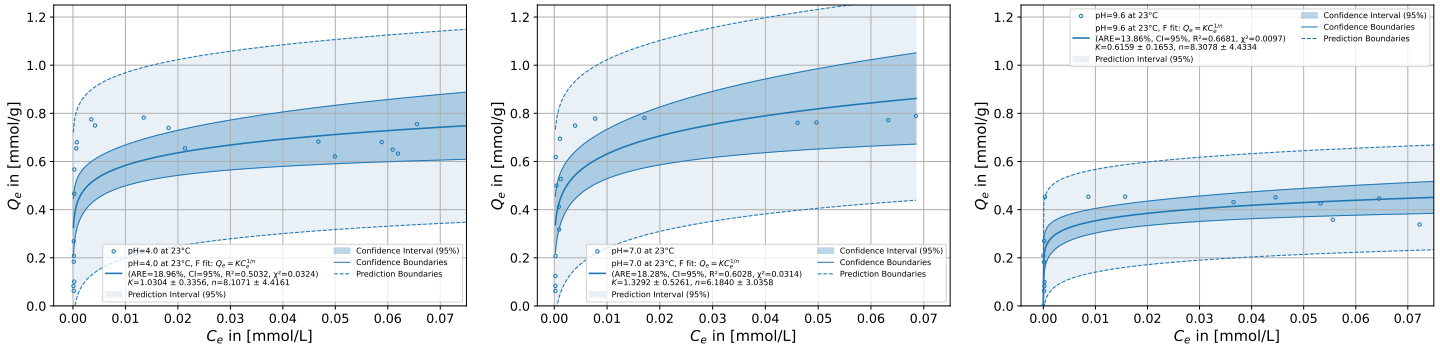

(a) pH=4.0 **(b)** pH=7.0 **(c)** pH=9.6

Fig. S14 Ofloxacin isotherms obtained by means of Freundlich model.

13.2 Results of Langmuir-Freundlich model for ofloxacin

We have also utilized the Langmuir-Freundlich model for modeling the ofloxacin adsorption data, as shown in Figure S15. The isotherms for pH 4.0, 7.0, and 9.6 are depicted in Figures S15a to S15c††. We chose the Langmuir model in this paper since its K coefficient can be linked to thermodynamic properties and offers a more physically meaningful interpretation of the adsorption phenomenon. We note that the main scope of this work is not to determine the best fitting model for ofloxacin adsorption.

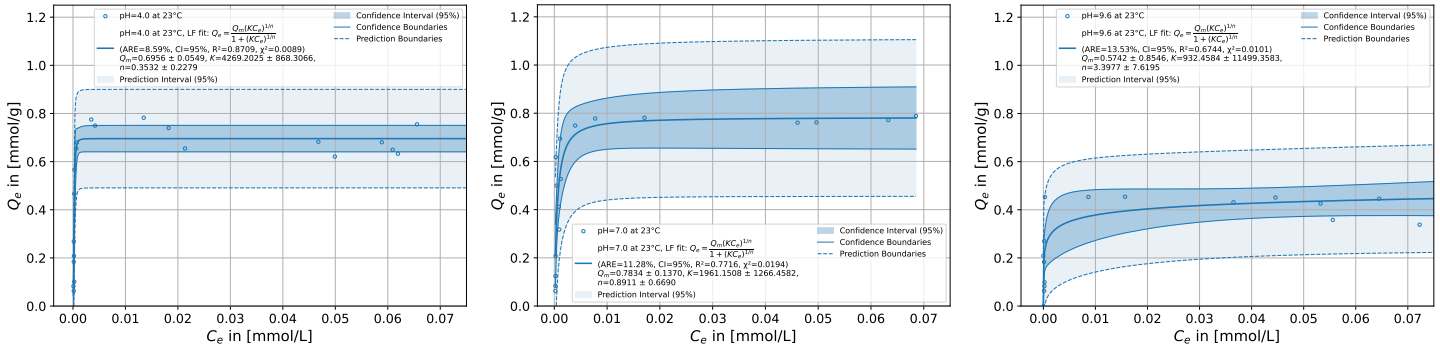

(a) pH=4.0 **(b)** pH=7.0 **(c)** pH=9.6

Fig. S15 Ofloxacin isotherms obtained by means of Langmuir-Freundlich model.

14 Electronic density and electric field lines of all ofloxacin forms

Besides the dipole moment vector, which is calculated and illustrated in Figure 11 via DFT computations, we have also calculated the electron density of all ofloxacin forms as shown in Figure S16, along with the electrostatic field lines. The blue-white-red color scheme is used to visualize both electron density and field lines. The red color represents negative values and the blue color represents positive values, using the BWR color scheme of VMD [17,40].

As shown in Figure S16a, the neutral form of ofloxacin has a weak electrostatic field compared to the other forms (Figures S16b to S16d). Figure S16b shows negative electron density (red coloring), whereas the acidic case exhibits very positive electron density (Figure S16c). For the zwitterionic form (Figure S16d), both strong positive and negative electron densities and field lines can be observed, indicating its high dipole moment compared to the other forms of ofloxacin.

†† We note that ARE stands for Average Relative Error [38], R^2 signifies the correlation coefficient, and χ^2 represents the nonlinear Chi-Square Test [37,39].

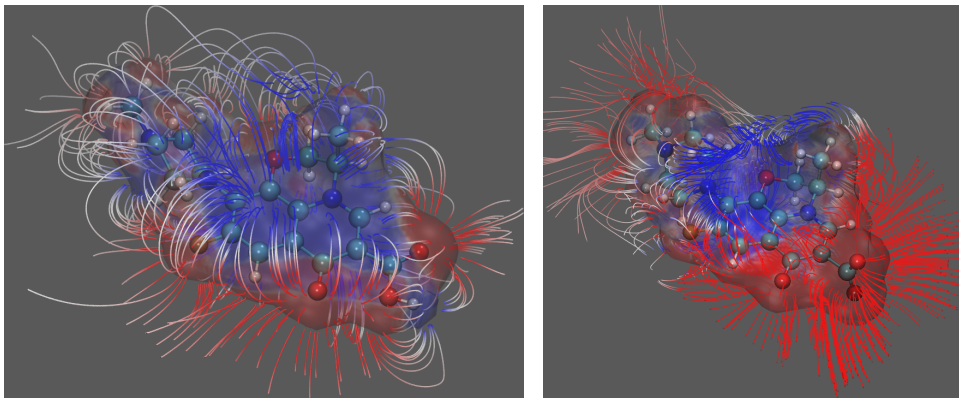

(a) HQ^0 (Neutral form) **(b)** Q^- (basic form)

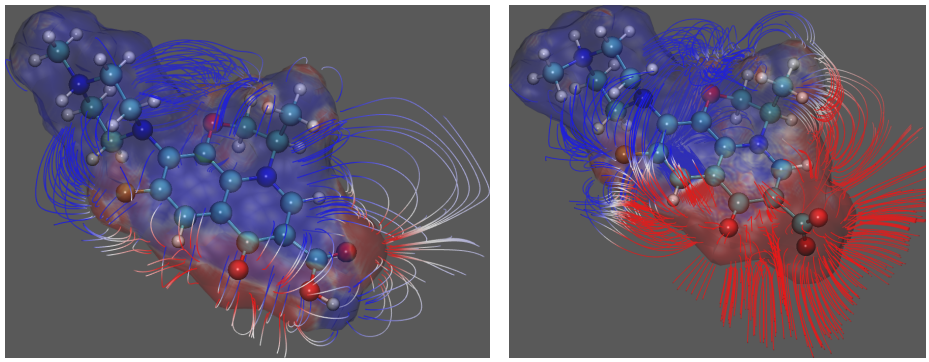

(c) H_2Q^+ (acidic form) **(d)** $HQ^\pm$ (zwitterionic form)

Fig. S16 Electron density and electric field lines of all ofloxacin forms (blue-white-red color scheme).

15 Ofloxacin conformers

15.1 Basic assumptions and calculations

Conformers can be calculated using both DFT and generator methods such as RDKit. Since DFT calculations are computationally expensive for finding all possible conformers and selecting the most stable ones, we use the generator method with an energy threshold of 0.05 kcal/mol and an RMSD (Root Mean Square Deviation) threshold of 0.125. This approach avoids computational burden during calculations while still providing satisfactory results [18].

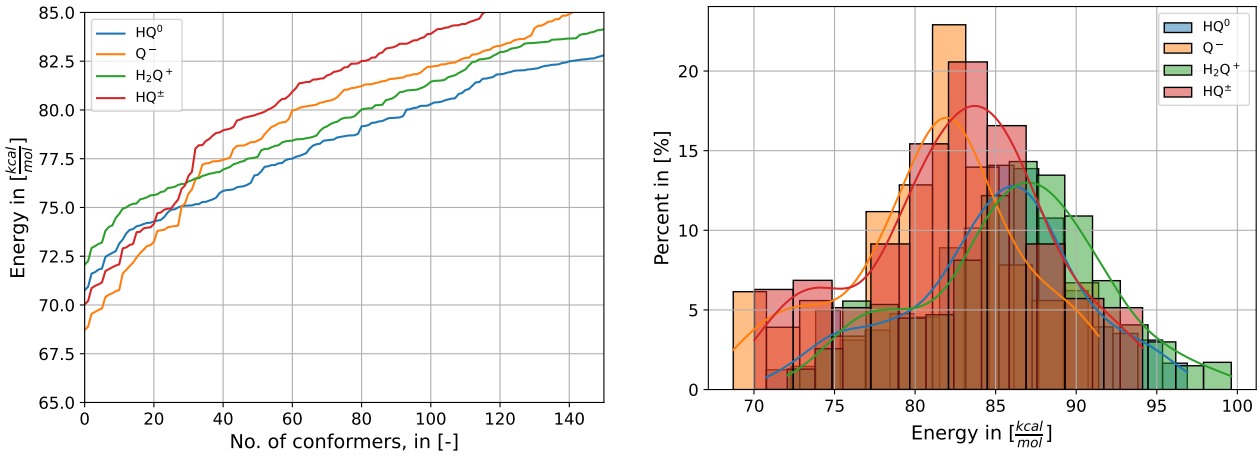

(a) **(b)**

Fig. S17 Conformer energy versus number of conformers and probability distribution versus energy.

15.2 Conformation results

The results of these computations are shown in Figure S17. Figure S17a plots the energy as a function of the number of explored conformations. We examined up to 500 conformers and here report only the first 150 stable ones. At first glance, the basic form of ofloxacin (Q^-) appears most stable, followed by the zwitterionic form ($HQ^{\pm}$), the neutral form (HQ^0), and the acidic form (H_2Q^+). However, the lowest energy conformers of each form lie very close in energy, ranging from 68 kJ/mol to 72 kJ/mol.

Snapshots of the four most stable conformers of the neutral, basic, acidic, and zwitterionic forms are shown in Figures S18 to S21. Figure S17 shows the conformer energy as a function of the number of conformers, along with the probability distribution of their energies. In Figure S17b, the data from Figure S17a are represented as a probability distribution, again highlighting the energy ordering ($Q^- > HQ^{\pm} > HQ^0 > H_2Q^+$). Studying the conformers of flexible large molecules is particularly important because their ability to adopt multiple shapes facilitates docking onto adsorbent surfaces, as shown elsewhere[16]. Comparison of the neutral form conformers in Figure S18 reveals only very small differences among them. This limited flexibility arises from the rigid quinolones aromatic system of ofloxacin, whereas diclofenac can rotate more freely about the axis that connects its aromatic rings. Overall, the same trend holds for ofloxacin's basic form (Figure S19), acidic form (Figure S20), and zwitterionic form (Figure S21).

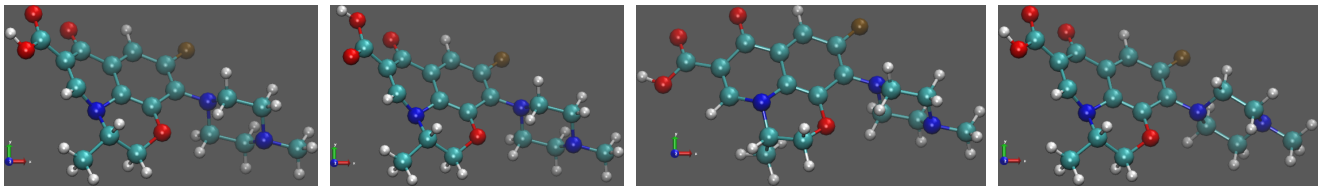

(a) E=70.75 kcal/mol **(b)** E=70.93 kcal/mol **(c)** E=71.61 kcal/mol **(d)** E=71.68 kcal/mol

Fig. S18 Four most stable conformers of neutral form of ofloxacin (HQ^0).

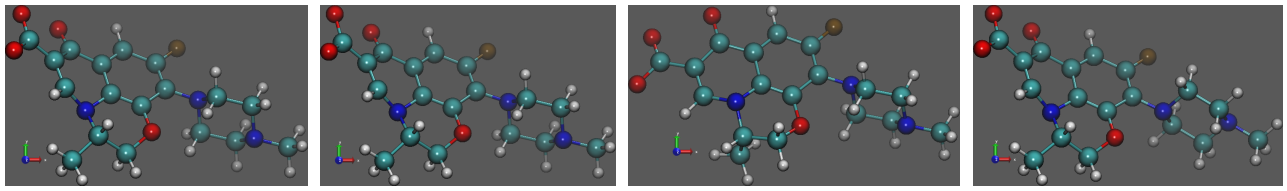

(a) E=68.71 kcal/mol **(b)** E=68.88 kcal/mol **(c)** E=69.55 kcal/mol **(d)** E=69.64 kcal/mol

Fig. S19 Four most stable conformers of anionic form of ofloxacin (Q^-).

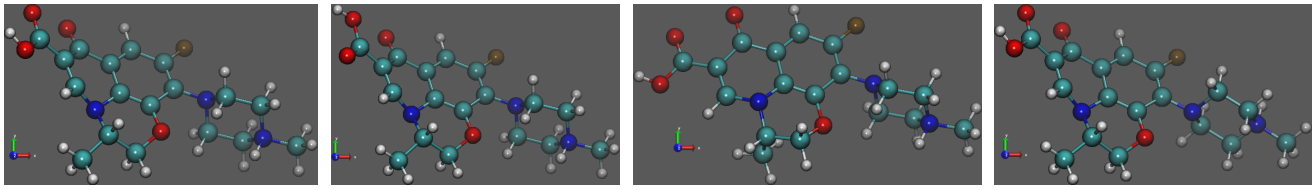

(a) E=72.07 kcal/mol **(b)** E=72.25 kcal/mol **(c)** E=72.92 kcal/mol **(d)** E=73.02 kcal/mol

Fig. S20 Four most stable conformers of cationic form of ofloxacin (H_2Q^+).

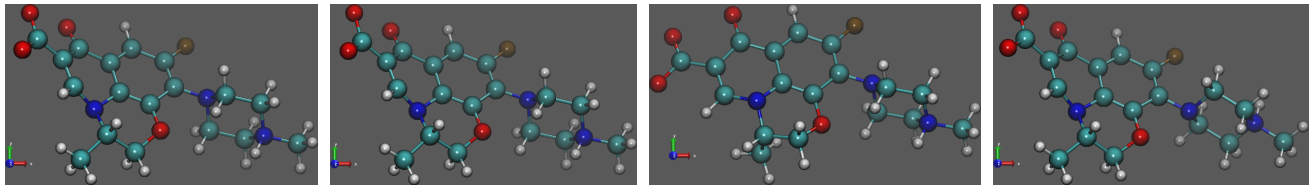

(a) E=70.03 kcal/mol **(b)** E=70.20 kcal/mol **(c)** E=70.86 kcal/mol **(d)** E=70.98 kcal/mol

Fig. S21 Four most stable conformers of zwitterionic form of ofloxacin ($HQ^{\pm}$).

Supplementary References

1 A. H. Farmahini, G. Opletal and S. K. Bhatia, *The Journal of Physical Chemistry C*, 2013, **117**, 14081–14094.

2 T. X. Nguyen, N. Cohaut, J.-S. Bae and S. K. Bhatia, *Langmuir*, 2008, **24**, 7912–7922.

3 J. C. Palmer, S. J. Jain, K. E. Gubbins, N. Cohaut, J. E. Fischer, R. K. Dash and Y. Gogotsi, Proceedings of the 8th International Symposium on the Characterisation of Porous Solids, 2009, pp. 1–8.

4 W. A. Steele, *The Journal of Physical Chemistry*, 1978, **82**, 817–821.

5 L. Liu, D. Nicholson and S. K. Bhatia, *Carbon*, 2017, **125**, 245 – 257.

6 D. Nguemalieu Kouetcha, *PhD thesis*, Université d'Orléans, 2017.

7 H. J. C. Berendsen, J. R. Grigera and T. P. Straatsma, *The Journal of Physical Chemistry*, 1987, **91**, 6269–6271.

8 U. W. Schmitt and G. A. Voth, *The Journal of Chemical Physics*, 1999, **111**, 9361–9381.

9 S. Izadi and A. V. Onufriev, *The Journal of Chemical Physics*, 2016, **145**, 074501.

10 K. S. Smirnov, *Physical Chemistry Chemical Physics*, 2017, **19**, 2950–2960.

11 S. Izadi, R. Anandakrishnan and A. V. Onufriev, *The Journal of Physical Chemistry Letters*, 2014, **5**, 3863–3871.

12 W. L. Jorgensen, J. Chandrasekhar, J. D. Madura, R. W. Impey and M. L. Klein, *The Journal of Chemical Physics*, 1983, **79**, 926–935.

13 H. W. Horn, W. Swope, J. W. Pitera, J. D. Madura, T. J. Dick, G. L. Hura and T. Head-Gordon, *The Journal of chemical physics*, 2004, **120**, 9665–78.

14 M. A. González and J. L. F. Abascal, *The Journal of Chemical Physics*, 2011, **135**, 224516.

15 M. T. Humbert, Y. Zhang and E. J. Maginn, *Journal of Chemical Information and Modeling*, 2019, **59**, 1301–1305.

16 A. Richard, F. A. Camara, H. Ramézani, N. Mathieu, S. Delpeux and S. K. Bhatia, *Colloids and Surfaces A: Physicochemical and Engineering Aspects*, 2024, **686**, 133373.

17 W. Humphrey, A. Dalke and K. Schulten, *Journal of Molecular Graphics*, 1996, **14**, 33 – 38.

18 G. te Velde, F. M. Bickelhaupt, E. J. Baerends, C. Fonseca Guerra, S. J. A. van Gisbergen, J. G. Snijders and T. Ziegler, *Journal of Computational Chemistry*, 2001, **22**, 931–967.

19 A. P. Thompson, H. M. Aktulga, R. Berger, D. S. Bolintineanu, W. M. Brown, P. S. Crozier, P. J. in 't Veld, A. Kohlmeyer, S. G. Moore, T. D. Nguyen, R. Shan, M. J. Stevens, J. Tranchida, C. Trott and S. J. Plimpton, *Comp. Phys. Comm.*, 2022, **271**, 108171.

20 O. R. Gittus and F. Bresme, *The Journal of Chemical Physics*, 2021, **155**, 114501.

21 F. A. Camara, H. Ramézani, N. Mathieu, S. Delpeux-Ouldriane and S. K. Bhatia, *Langmuir*, 2025, **41**, 3334–3355.

22 R. T. Hanlon, in *Practical applications and Gibbs energy (G)*, Oxford University PressOxford, 2020, pp. 514–520.

23 C. H. Bennett, *Journal of Computational Physics*, 1976, **22**, 245–268.

24 V. Khanna, J. I. Monroe, M. F. Doherty and B. Peters, *Journal of Computer-Aided Molecular Design*, 2020, **34**, 641–646.

25 Z. El Oufir, *PhD thesis*, CNRS, ICMN, UMR 7374, Université d'Orléans, 2020.

26 R. Weiss, *Marine Chemistry*, 1974, **2**, 203 – 215.

27 M. Allen and D. Tildesley, *Computer simulation of liquids*, Clarendon Press, 1989.

28 D. Frenkel and B. Smit, *Understanding molecular simulation: from algorithms to applications*, Academic Press, 2002.

29 J. H. Dymond, K. N. Marsh, R. C. Wilhoit and K. C. Wong, *Virial Coefficients of Pure Gases and Mixtures*, Springer Berlin Heidelberg, 2002.

30 J. M. H. L. Sengers, M. Klein and J. S. Gallagher, *Pressure-Volume-Temperature Relationships of Gases- Virial Coefficients*, U.S. Air Force Technical Report 197108, 1971.

31 I. Langmuir, *Journal of the American Chemical Society*, 1918, **40**, 1361–1403.

32 S. Masson, *Theses*, Université Grenoble Alpes, 2015.

33 S. Masson, L. Reinert, S. Guittonneau and L. Duclaux, *Revue des sciences de l'eau / Journal of Water Science*, 2015, **28**, 207–213.

34 S. Delpeux-Ouldriane, M. Gineys, N. Cohaut, F. Béguin, S. Masson, L. Reinert and L. Duclaux, *International Journal of Environmental Pollution and Remediation (IJEPR)*, 2016, **4**, 1–6.

35 H. Freundlich, *Zeitschrift für Physikalische Chemie*, 1907, **57U**, 385–470.

36 R. Sips, *The Journal of Chemical Physics*, 1948, **16**, 490–495.

37 N. Ayawei, A. N. Ebelegi and D. Wankasi, *Journal of Chemistry*, 2017.

38 D. Saha, K. Nelson, J. Chen, Y. Lu and S. Ozcan, *Journal of Chemical & Engineering Data*, 2015, **60**, 2636–2645.

39 R. Vitek and J. C. Masini, *Heliyon*, 2023, **9**, e15128.

40 N. A. Baker, D. Sept, S. Joseph, M. J. Holst and J. A. McCammon, *Proceedings of the National Academy of Sciences*, 2001, **98**, 10037–10041.